Analysis of the total $^{12}C(\alpha,\gamma)^{16}O$ cross section based on available angular distributions and other primary data

L. Buchmann,[1] R.E. Azuma,[2] C.A. Barnes,[3] J. Humblet,[3,4] and K. Langanke[3]
[1]*TRIUMF, 4004 Wesbrook Mall, Vancouver, British Columbia, Canada V6T 2A3*
[2]*Department of Physics, University of Toronto, Toronto, Ontario, Canada M5S 1A7*
[3]*W. K. Kellogg Radiation Laboratory, California Institute of Technology, Pasadena, California 91125*
[4]*University of Liège, Institute of Physics B5, 4000 Liège, Belgium*
(Received 7 March 1996)

Because a knowledge of the $^{12}C/^{16}O$ ratio is crucial to the understanding of the later evolution of massive stars, new R- and K-matrix fits have been completed using the available angular distribution data from radiative α capture and elastic α scattering on ^{12}C. Estimates of the total $^{12}C(\alpha,\gamma)^{16}O$ rate at stellar energies are reported. In contrast with previous work, the analyses generally involve R- and K-matrix fits directly to the primary data, i.e., the energy- and angle-dependent differential yields, with all relevant partial waves fitted simultaneously (referred to here as surface fits). It is shown that, while the $E1$ part of the reaction is well constrained by a recent experiment on the β-delayed α-particle decay of ^{16}N, only upper limits can be placed on the $E2$ ground state cross section factor which we take conservatively as $S_{E2}(300)<140$ keV b. Simulations were then carried out to explore what kind of new data could lead to better restrictions on $S_{E2}(300)$. We find that improved elastic scattering data may be the best short-term candidate for such restrictions while significantly improving $S(300)$ with new radiative capture data may require a longer-term effort. Theoretical models and estimates from α-transfer reactions for the $E2$ part of $^{12}C(\alpha,\gamma)^{16}O$ are then discussed for comparison with the R- and K-matrix fits of the present work. [S0556-2813(96)03307-9]

PACS number(s): 27.20.+n, 25.55.−e, 26.20+f

I. INTRODUCTION

In the helium-burning phase of massive stars only two nuclear reactions are of essential importance: the triple-α reaction leading to the production of ^{12}C and the subsequent $^{12}C(\alpha,\gamma)^{16}O$ reaction [1–3]. The ratio of these two reaction rates determines the $^{12}C/^{16}O$ ratio after helium burning and consequently both the amounts of ^{12}C and ^{16}O, and of the heavier nuclides built from these nuclei. In addition, the further structural evolution of the star is influenced by the ratio of carbon to oxygen, resulting in different iron core masses before the onset of the final supernova collapse and explosion, which will, in turn, affect the relative probabilities of different types of supernova remnants [2,4].

While the triple-α reaction appears to be experimentally well determined, the situation is different for the $^{12}C(\alpha,\gamma)^{16}O$ reaction. Because the value of the cross section is required near the astrophysically most important energy $E=300$ keV,[1] theoretical extrapolations of the cross sections measured at higher energies are needed. In attempts to improve the reliability of the extrapolations, data from complementary experiments [$^{12}C(\alpha,\alpha)^{12}C$ elastic scattering and the earlier ^{16}N experiments] were included in the extrapolations. Initially these analyses did not improve the extrapolations. Values ranging from essentially 0 to 500 keV b were quoted for the S factor at $E=300$ keV [5–11]. It became apparent in these analyses that a major difficulty lay in the insensitivity of the higher-energy data (at the statistical level of the experiments) to the values of the reduced α widths of the $J^\pi=1^-$ and $J^\pi=2^+$ subthreshold states of ^{16}O at excitation energies $E_x=7.12$ MeV and 6.91 MeV, respectively. However, with the recent precise measurement of the β-delayed α-particle decay of ^{16}N [12], where it has been demonstrated that the α spectrum is quite sensitive to the reduced α width of the subthreshold $J^\pi=1^-$ state, the $E1$ radiative capture part of the $^{12}C(\alpha,\gamma)^{16}O$ reaction has been determined to about 30%. Nevertheless, the $E2$ part of this reaction remains poorly determined partly because no model-independent alternative measurement for the reduced width of the $J^\pi=2^+$ state has become available. The same is true for cascade transitions in the radiative capture, though these are less important at stellar energies.

However, in recent network calculations of nucleosynthesis in massive stars [2], the results are found to be in excellent agreement with solar system abundances for all the intermediate masses ($16\leqslant A\leqslant 32$) if the S factor[1] for the $^{12}C(\alpha,\gamma)^{16}O$ reaction is 170 ± 50 keV b at 300 keV. This exceptionally tight restraint underlines the unusual sensitivity of stellar models to the total cross section of this reaction and implies that experiments of better than 30% precision are required for a definitive test of theories of stellar evolution.

In this work, we explore the extent to which the available data may place further restrictions on the $E2$ part of the $^{12}C(\alpha,\gamma)^{16}O$ reaction after the $E1$ part has been determined, and to what extent future experiments may impose more stringent ones.

II. APPROACHES TO THE ANALYSIS

In the previous publications, as exemplified by Ref. [12], secondary data were in general used for both the radiative

[1]Throughout the paper E denotes center-of-mass energy and E_α represents laboratory α energy in the $\alpha+^{12}C$ system. The cross section factor $S(E)$ is defined by the relation $S(E)=E\sigma(E)\exp[2\pi\eta]$, where the Sommerfeld parameter $\eta=Z_1Z_2\alpha[\mu c^2/2E]^{1/2}$.

capture and elastic scattering aspects of the analyses. In both cases the primary data most often consisted of angular distributions measured at many discrete energies (see Secs. III B 1 and III B 2 for details). Each primary distribution was then analyzed independently in terms of the appropriate set of Legendre polynomials to yield the secondary data consisting of the relevant angular momentum components. In the case of radiative capture, the secondary data consisted of sets of derived σ_{E1} and σ_{E2} cross sections, while for the elastic scattering the secondary data were comprised of sets of phase shifts δ_ℓ for $\ell=0$–6. It was at this stage in the previous work that R- and K-matrix fits were introduced in the analysis of the secondary data. In all cases, experimental errors were propagated to yield errors for the derived data. However, these data and their error values, being derived quantities, are no longer proportional to the experimentally measured quantities, i.e., the angular distribution yields, and thus lead to complications for the interpretation of the statistical and systematic errors of the experiment and analysis.

In work preparatory to extending the analysis of the available data to include the $E2$ part of the radiative capture, we have reanalyzed the original primary angular distributions for both the radiative capture and elastic scattering experiments. In doing so, we have found that the angular momentum components were highly correlated. The use of the separate, derived angular momentum data sets as independent data in subsequent R- and K-matrix analyses, as was done previously, may therefore have introduced significant errors.

In addition to these problems with correlations between the partial waves, problems are introduced when the analysis of each angular distribution is carried out independently from those at the other energies. The coefficients in the Legendre polynomial expressions for the angular distributions are the energy-dependent cross sections for the radiative capture or are functions of the phase shifts for the elastic scattering. The energy dependence of these quantities has been ignored in all previous analyses of the angular distributions in which the quantities themselves were treated as independent adjustable parameters for the analysis at each energy. This would be a reasonable approach if the energy dependence were very slowly varying, and if systematic energy-dependent errors were negligible. It is likely, however, that energy-dependent systematic errors are the major source of uncertainty in both types of experiment, and at least in the case of the elastic scattering, the differential cross sections vary extremely rapidly over the whole energy range of the experiments. This possible energy dependence of systematic problems will become apparent in the discussion of the elastic data (Sec. III C 3).

The present reanalysis of the angular distribution data has shown that the previous approaches very often led to least squares fits for which the reduced χ^2 values were significantly less than unity. If, on the other hand, the data are presented as functions of energy (i.e., yield versus energy for each specific angle), then much larger fluctuations and systematic errors became evident. Also, in the case of the elastic scattering angular distributions where the yields vary rapidly with energy, an integration over finite target thickness is necessary. This cannot be accomplished without taking the energy dependence of the cross sections into account. In this connection it will be shown below (Sec. III B 2) that individual Legendre polynomial fits to the primary data can incorrectly compensate for target-thickness-induced effects.

In order to illustrate these considerations, the relevant angular distributions are presented below with the energy dependence explicitly indicated.

For radiative capture we use [9]

$$\begin{aligned} W(\theta_\gamma,E)=&1-Q_2P_2(\cos\theta_\gamma)+[\sigma_{E2}(E)/\sigma_{E1}(E)]\\ &\times[1+\tfrac{5}{7}Q_2P_2(\cos\theta_\gamma)-\tfrac{12}{7}Q_4P_4(\cos\theta_\gamma)]\\ &+\tfrac{6}{5}[5\sigma_{E2}(E)/\sigma_{E1}(E)]^{1/2}\cos\Phi(E)\\ &\times[Q_1P_1(\cos\theta_\gamma)-Q_3P_3(\cos\theta_\gamma)], \end{aligned} \tag{1}$$

where $P_k(\cos\theta_\gamma)$ are the Legendre polynomials in the center-of-mass system, Q_k the experimental attenuation coefficients of the γ detectors, and $\Phi(E)$ the phase difference between the p and d waves. The phase difference angle $\Phi(E)$ is given in general scattering theory by

$$\Phi(E)=\delta_2(E)-\delta_1(E)+\arctan(\tfrac{1}{2}\eta), \tag{2}$$

with η being the Sommerfeld parameter. This expression has been used throughout for $\Phi(E)$ with the elastic phase shifts δ available from experiment.

The elastic phase-shift analysis is performed using the single-channel, spin-zero formula of Refs. [13–15],

$$\begin{aligned} \frac{d\sigma(\theta_\alpha,E)}{d\Omega}=&\frac{1}{k^2}\left|-\frac{\eta}{2}\sin^{-2}\left(\frac{1}{2}\theta_\alpha\right)\exp\left[-2i\eta\ln\sin\left(\frac{1}{2}\theta_\alpha\right)\right]\right.\\ &+\sum_{\ell=0}^{\infty}(2\ell+1)P_\ell(\cos\theta_\alpha)\exp\{i[2\alpha_\ell+\delta_\ell(E)]\}\\ &\left.\times\sin\delta_\ell(E)\right|^2, \end{aligned} \tag{3}$$

with the Coulomb phases

$$\alpha_\ell=\sum_{m=1}^{\ell}\arctan\frac{\eta}{m},\quad \alpha_0=0. \tag{4}$$

It is evident from these expressions that both $W(\theta_\gamma,E)$ and $d\sigma(\theta_\alpha,E)/d\Omega$ represent surfaces above the (θ_γ,E) and (θ_α,E) planes for which the energy-dependent cross sections and phase shifts can be expressed in terms of a common set of R- or K-matrix parameters. The experimental angular distributions upon which the previous analyses were based are obviously cuts $E=$const through these surfaces. In the present study, however, a more comprehensive analysis is carried out which includes fits over the entire surface of each set of distributions. In this way, the fits are made directly to the primary data, and all the angular momentum components (e.g., σ_{E1}, σ_{E2}, and δ_ℓ) are treated equally, consistently, and simultaneously in terms of the R- and K-matrix parameters. Fits of this type are referred to as *surface fits* throughout the rest of this report.

In the present work we have thus performed an analysis mainly of the primary data available in the literature including the data recently reported in Ref. [11] for which only a preliminary account has been published. Unfortunately, the kind of primary data required in our analysis cannot be extracted from all of the published measurements of the $^{12}C(\alpha,\gamma)^{16}O$ reaction; in particular the measurements of Refs. [9] and [10] could not be analyzed by the approach used in this work as discussed in Sec. III B 1. However, to maintain a connection with the previous analyses, and for comparison purposes, we also perform some fits to secondary data.

The paper has the following structure: After giving an overview of the theory and data used, R- and K-matrix fits to these data are discussed and an upper limit for $S_{E2}(300)$ is derived. After this step, the degree to which future improvements in experimental results could lead to improvements in our knowledge of the astrophysical S factor at $E=300$ keV [abreviated $S(300)$ in the following] for $^{12}C(\alpha,\gamma)^{16}O$ is discussed. To compare with our value of $S(300)$, theoretical optical-model calculations for $^{12}C(\alpha,\gamma)^{16}O$ are discussed. In addition, α-transfer data which may, in principle, determine the reduced width of the $E_x=6.917$ MeV state[2] in ^{16}O are introduced in our fits to obtain a comparison with our value of $S_{E2}(300)$. From this work we draw some conclusions regarding $S(300)$.

III. SURFACE R- AND K-MATRIX FITS TO AVAILABLE DATA

A. Formal approach used in the fits

The general R- and K-matrix approaches to the simultaneous analyses of the three kinds of data have been well documented in [12] and references therein. In these previous analyses only the $E1$ part of the $^{12}C(\alpha,\gamma)^{16}O$ reaction was included. Also, only the δ_1 and δ_3 experimental phase shifts [12,13] for the elastic scattering and the $\ell=1$ and $\ell=3$ components for the β-delayed α-spectrum of ^{16}N were used in the parametrization. In the present work we wish to extend the analysis of the radiative capture reaction to include the $E2$ component and the elastic scattering to include phase shifts from $\ell=0$ to $\ell=6$. All the necessary equations and notation are given in [12] except those for the $E2$ component of the radiative capture which are given in the next section.

Because of the more comprehensive analysis undertaken here, additional states are required for the present parametrizations. For the s wave ($\ell=0$) we use the 6.049 MeV subthreshold state and up to two background states.[3] We use three states (7.12 MeV, 9.61 MeV, and a $J^\pi=1^-$ background state) for the parametrization of the $\ell=1$ components of the radiative capture, the beta-delayed alpha decay of ^{16}N, and the elastic scattering. Similar considerations hold true for the $\ell=3$ partial waves of the β-delayed α decay of ^{16}N and the elastic scattering (i.e., states at 6.13 MeV, 11.4 MeV, and a $J^\pi=3^-$ background state). For the $\ell=2$ components, the radiative capture is parametrized in terms of a state at 6.91 MeV, a direct capture (DC) component (only R matrix), the 11.52 MeV state, and a $J^\pi=2^+$ background state, while the elastic scattering utilizes the same states at 6.91 MeV, 11.52 MeV, and the same $J^\pi=2^+$ background state. The $\ell=4$ elastic scattering is represented in terms of states at 10.356 MeV, 11.097 MeV, and a $J^\pi=4^+$ background state. The $\ell=5$ and $\ell=6$ phase shifts are given in terms of single $J^\pi=5^-$ and $J^\pi=6^+$ background states, respectively. Background pole terms in K-matrix theory can be either real or complex as discussed subsequently; echo poles were allowed as background terms. In addition, our K-matrix expressions contain a constant background term for $\ell=1$ and 2. As was done in [12], known values of the energies, as well as the α and γ widths for several of the states were taken from [16].

Because of the large number of states and different kinds of data involved, up to 48 parameters could be used in the full fits. However, some of them were kept constant, in particular experimentally related parameters, while the interaction radius a, which does not provide a straightforward minimization with our programs, was varied in fixed steps. It may also be noted that the number of parameters in fits to each individual distribution was far smaller. Because of the high number of parameters, the large number of fits, and the ambiguous results finally obtained, we do not give parameter tables in this paper; however, they are available from the authors on request.

The boundary conditions B_ℓ in R-matrix theory have been taken to be equal to the shift functions evaluated at the subthreshold state energies of the $\ell=0$, 2, and 3 waves; for the $\ell=1$ wave the matching energy was 300 keV as in Ref. [12], while for the $\ell=4$ wave the position of the $J^\pi=4^+$ resonance at 10.35 MeV was selected; 1 MeV was chosen arbitrarily for $\ell=5$ and 6. In the K-matrix theory additional constraints on the background terms for $\ell=2$ were introduced by using an optical potential model. As in Ref. [12] we convoluted the β-delayed α spectrum of ^{16}N with the detector resolution.

1. R-matrix formalism: E2 radiative capture

The extension of the R-matrix analysis to include the $E2$ radiative capture component is mainly based on the work of [17] and we give here a brief summary of the relevant formalism. Reference [17] in turn is based on Ref. [18]. This approach is derived from perturbation theory and assumes that there is no other strong-interaction channel open at low $\alpha+^{12}C$ scattering energies. The ^{16}O ground state is described by an $\alpha+^{12}C$ factorization with total angular momentum $J_f=0$ and a dimensionless reduced α width[4] $\theta_{\alpha f}$.

[2]For brevity, state energies in ^{16}O will be referred to in the following text by quoting their excitation energy without the symbol E_x, and without special reference to ^{16}O where there is no ambiguity.

[3]Variations beyond one background state for the s wave resulted in little change in the quality of the fits.

[4]In defining the dimensionless reduced α width θ_α we follow the convention of Ref. [19]. In part of the literature, e.g., Ref. [20], the definition of the reduced width differs from the one used here by a factor $\sqrt{3/2}$.

The $E2$ capture at low energies then occurs from $\alpha+{}^{12}$C scattering states with $J_i=\ell_i=2$.

The $E2$ capture cross section to the ground state is then given by [17]

$$\sigma_{20}=5\frac{\pi}{k^2}|U_{20}|^2, \tag{5}$$

where k is the wave number of the incoming particle and

$$|U_{20}|^2=4P_2k_\gamma^5\Big|\sum_{\lambda,\mu}\gamma_{\lambda\alpha}\gamma_{\mu\gamma}A_{\lambda\mu}+U_{\rm DC}\Big|^2. \tag{6}$$

In this expression P_2 is the penetrabilty for the incoming particle, $k_\gamma=E_\gamma/\hbar c$ is the photon wave number, and $\gamma_{\lambda\alpha}$ ($\gamma_{\mu\gamma}$) are the α-width (γ-width) amplitudes of the level $\lambda(\mu)$. The first part of the sum is a standard R-matrix expression where the inverse of the level matrix is given by

$$[(\boldsymbol{A_2})^{-1}]_{\lambda\mu}=(E_{2\lambda}-E)\,\delta_{\lambda\mu}-(S_2-B_2+iP_2)\,\gamma_{\lambda\alpha}\gamma_{\mu\alpha}, \tag{7}$$

where $\delta_{\lambda\mu}$ is the Kronecker delta symbol; the shift function S_2 and the boundary condition B_2 refer to the (elastic) α channel. Following Ref. [17], the photon reduced-width amplitude can be split into internal and asymptotic channel contributions:

$$\gamma_{\lambda\gamma}=\gamma_{\lambda\gamma}(\text{int})+\gamma_{\lambda\gamma}(\text{ch}), \tag{8}$$

where the first part is independent of energy, while the second part has a slight energy dependence,

$$\gamma_{\lambda\gamma}(\text{ch})=\sqrt{\frac{3}{2}}\Lambda a\,\theta_{\alpha f}\gamma_{\lambda\alpha}\left[J''(E)+i\frac{F_2G_2}{F_2^2+G_2^2}J'(E)\right], \tag{9}$$

with

$$\Lambda=\frac{3e}{\sqrt{50}}\frac{M^{1/2}}{\hbar}N_f^{1/2}a^2. \tag{10}$$

Here M is the reduced mass, e is the elementary charge, and N_f is the integral expression defined as

$$N_f^{-1}=1+\frac{3(\theta_{\alpha f})^2}{a}\int_a^\infty dr\left[\frac{W_0(r)}{W_0(a)}\right]^2. \tag{11}$$

In Eq. (9) the regular and irregular Coulomb functions F_2 and G_2 have to be determined at the interaction radius a. The Whittaker function $W_0(r)$ is the asymptotic part of the ^{16}O ground state wave function. The energy-dependent functions $J'(E)$ and $J''(E)$ are given by

$$J'(E)=\frac{1}{a^3}\int_a^\infty drr^2\frac{W_0(r)}{W_0(a)}\left[\frac{F_2(r)}{F_2(a)}-\frac{G_2(r)}{G_2(a)}\right] \tag{12}$$

and

$$J''(E)=\frac{1}{a^3}\int_a^\infty drr^2\frac{W_0(r)}{W_0(a)}\,\frac{F_2(a)F_2(r)+G_2(a)G_2(r)}{F_2^2(a)+G_2^2(a)}. \tag{13}$$

We note that in Eq. (8) two related γ-width parameters per state λ have been introduced into the fitting procedure. Because the energy dependence of $\gamma_{\lambda\gamma}$(ch) is rather weak, we therefore chose to use only one γ-width parameter, i.e., setting $\gamma_{\lambda\gamma}$(int) to zero. Then, to match $\gamma_{\lambda\gamma}$ to the known γ width of the 6.917 MeV state in ^{16}O (Γ_γ=97 meV [16]), it is necessary to extrapolate $\gamma_{\lambda\gamma}^2$(ch), and hence $J'(E)$ and $J''(E)$ to $E=-0.245$ MeV. Tests with a constant $\gamma_{\lambda\gamma}$ show little difference in the final fitting results.

Finally, the direct capture expression $U_{\rm DC}$ in Eq. (6) is given by

$$U_{\rm DC}=\sqrt{\frac{3}{2}}\frac{\Lambda}{k}F_2(a)G_2(a)\,\theta_{\alpha f}J'(E). \tag{14}$$

2. K-matrix formalism: E2 radiative capture

Because the K-matrix formalism makes no explicit reference to channel radii, it has no prescription for separate inclusion of hard core terms and direct radiative capture terms. On the other hand, the formalism requires that both bound states and resonances be described by pole structures in all channels [21–23]. We have attempted to reduce any uncertainty in the form of the K-matrix background parametrization by analyzing the results of a microscopic potential model simulation of the $E2$ capture process ([9] and Secs. III C 1, III C 4, and V D). We find that, in the relevant energy region ($E\leqslant 2.5$ MeV), the background in the simulated capture cross section is well reproduced by the sum of a constant background term B and an echo pole at $E\approx 8$ MeV, in agreement with the background parametrization adopted in Ref. [23]. For consistency we then adopted the same parametrization and energy range for the elastic phase-shift data. Thus our K-matrix parametrization (in the notation of Refs. [21,23]) reads

$$\mathcal{K}_{\alpha\gamma}=\frac{g_{\alpha1}g_{\gamma1}}{E_1-E}+\frac{g_{\alpha2}g_{\gamma2}}{E_2-E}+B_{\alpha\gamma}, \tag{15}$$

$$\mathcal{K}_{\alpha\alpha}=\frac{g_{\alpha1}g_{\alpha1}}{E_1-E}+\frac{g_{\alpha2}g_{\alpha2}}{E_2-E}+B_{\alpha\alpha}, \tag{16}$$

where the subscripts (1,2) refer to the subthreshold 2^+ state and echo pole, respectively, and the background parameters $B_{\alpha\gamma}$,$B_{\alpha\alpha}$ are constants.

As found in Ref. [23], Eqs. (15) and (16) provide a good fit to the radiative capture, and the elastic phase-shift data of Ref. [13]. Similarly, good fits were obtained employing the elastic scattering angular distribution data. We also verified with K-matrix fits that the target thickness dependence of the elastic data is independent of the formalism (see Fig. 6). Nevertheless, because of possible uncertainties in the low-energy elastic scattering data (see Sec. III C 3), fits involving the full set of elastic scattering angular distribution data have not been pursued further with the K-matrix formulation.

As has been discussed in Ref. [23], $S_{E2}(300)$, the $E2$ cross-section S factor at 300 keV, is highly correlated with the reduced α width of the bound 2^+ level. We have therefore incorporated $S_{E2}(300)$ in place of the reduced α width $g_{\alpha1}$ of the 6.917 MeV state in our K-matrix parametrization.

This was also done for the R-matrix parameter sets.[5] In addition, as described in Ref. [12], $S_{E1}(300)$ has been substituted for the subthreshold α width of the 7.12 MeV state in both K- and R-matrix approaches.

B. Use of data and discussion of errors

1. Review of the literature on radiative α capture and the ^{16}N decay

There are many measurements of the $^{12}C(\alpha,\gamma)^{16}O$ cross section reported in the literature [5,6,8–11]. The early measurements of Refs. [5,6] show, however, such strong systematic differences from the rest of the data that we do not include them in the present fits. The remaining measurements fall into two categories: those where the primary angular distribution data are available [7,8,11] and those where only derived data (σ_{E1} and/or σ_{E2}) have been published [9,10]. Of those studies where the primary angular distribution data are available, Ref. [7] reports a set of measurements, at a sequence of energies, of the $^{12}C(\alpha,\gamma)^{16}O$ cross section with a large NaI(Tl) detector positioned at 90°. In addition, angular distributions at ten angular positions were obtained for four representative energies. The 90° measurements, from which a theoretical $E2$ part has been subtracted, are reported in Ref. [7] as the total $E1$ cross section. Because of the finite detector angular resolution and the model dependence of the subtraction, the primary data [24], from which these results were deduced, are treated as one point angular distributions in the fits.

In another study, Ref. [8] reports a measurement of the $^{12}C(\alpha,\gamma)^{16}O$ cross section in close geometry with a helium gas target in inverted kinematics. Because the geometry is close to an angle-integrated one and the detector attenuation factors are hard to construct from the publication, the cross section is assumed to be angle integrated.

Finally, Ref. [11] reports a measurement of the $^{12}C(\alpha,\gamma)^{16}O$ cross section using six germanium detectors, an α beam, and ^{12}C-implanted targets. Sixteen angular distributions at a variety of energies between $E=1.4$ MeV and 3.0 MeV are reported. This is the most detailed and complete set of primary angular distributions that are available in the literature, and hence one of the mainstays of the present analysis.

In summary, the 16 angular distributions of Ref. [11], the 4 angular distributions and the 17 90° measurements of Ref. [7], the 36 angle-integrated results of Ref. [8], and the 4 relative angular distribution measurements of Ref. [9] constitute the complete set of γ-ray angular distributions chosen for this new analysis.

Of those experiments where the primary data are not available, particularly extensive and thorough sets of angular distribution measurements are described in [9]. One set of measurements utilized eight NaI(Tl)detectors,[6] while two others employed six and three germanium detectors, respectively. Unfortunately the original angular distribution data cannot be reconstructed from the published material because only σ_{E1} and σ_{E2} and their ratios are available. In [9] the $E1$ values were derived by correcting the 90° detector data for a small $E2$ contribution due to the finite size of the detector. Values for σ_{E2} were then determined from fits made to each angular distribution using Eq. (2) where the relative phase $\Phi(E)$ was assumed to be an unconstrained fitting variable. Since the phase difference $\Phi(E)$ can be determined explicitly from Eq. (2) with the use of previously published phase-shift data, and since its value should vary in a continuous and known manner as a function of energy, it may be more appropriate to use Eq. (2) to calculate $\Phi(E)$. This was done in all the relevant fits described below.

In the second study of this category, Ref. [10] reports a measurement of the $^{12}C(\alpha,\gamma)^{16}O$ cross section using a ^{12}C beam, NaI detectors in close geometry, and a ^{16}O recoil detector. The analysis used a technique based largely on the σ_{E1}/σ_{E2} results of Ref. [9] to separate the $E1$ and $E2$ fractions of the $^{12}C(\alpha,\gamma)^{16}O$ cross section. While it may be possible to construct the original experimental yields from the published data, the information available is insufficient to derive the necessary angular acceptance corrections for the recoil detector.

There are three published papers on the β-delayed α spectrum of ^{16}N [25,26,12]. A critique of the published data of [25] can be found in [12]. In Ref. [26] the measurement of a low-statistics β-delayed α spectrum of ^{16}N has been reported. Because of the low statistical database, these results have not been incorporated into the fits. Therefore only the β-delayed α spectrum of ^{16}N reported in Ref. [12] is included in the present study.

2. Review of the literature on elastic scattering

In the measurements of elastic α scattering on ^{12}C only Ref. [13] reports useful primary angular distribution data. Additional angular distributions are shown in Refs. [14,15], but since they are reported without errors, they are excluded from the present analysis. In the work of [13] the angular distributions were analyzed using Eq. (3) (''Legendre fit'') for each individual distribution. We have repeated this analysis and find general agreement with the reported phase shifts. However, the (1σ) errors derived with the minimization routine[7] MINUIT [27] in our analysis are about a factor of 2 smaller for individual data points than those in Ref. [13], taking the quoted systematic errors into account. More importantly, from Figs. 9 and 10 of Ref. [13] it is obvious that there are strong correlations between partial waves. For example, between $E_\alpha=5.2$ and 5.8 MeV, corresponding to the broad 11.4 MeV 3^- resonance in ^{16}O, the $\ell=1$ data are noticeably lowered. The correlations between the partial waves were corroborated in the present analysis. The correlation matrix for such a Legendre fit [Eq. (3)] is shown, as an example, in Table I for the angular distribution at $E_\alpha=3.276$ MeV. This particular distribution was obtained on

[5]For computing time reasons this approach was abandoned in the R-matrix analyses when $S_{E2}(300)$ was not the subject of interest in a fit.

[6]The $E2$ cross sections derived from the NaI detectors are systematically larger by a factor of 2–3 than the other data and have therefore been disregarded in the following analyses.

[7]In general, for fitting minimizations, MINUIT was used. Tests with DNL2SN of the National Institute of Standards libraries gave nearly identical or slightly worse results.

TABLE I. Correlation matrix for a phase-shift fit according to Eq. (3) to the angular distribution at E_α=3.276 MeV of Ref. [13].

	δ_0	δ_1	δ_2	δ_3
δ_0	1.000	−0.214	−0.456	−0.461
δ_1	−0.214	1.000	0.908	0.942
δ_2	−0.456	0.908	1.000	0.931
δ_3	−0.461	0.942	0.931	1.000

the 9.61 MeV $J^\pi=1^-$ resonance where the fit should be dominated by the $\ell=1$ partial wave. However, Table I shows extremely strong correlations between the extracted $\ell=1,2,3$ phase shifts.

With regard to the target thickness problems alluded to above (Sec. II), Fig. 1 shows an angular distribution of Ref. [13] obtained at E_α=3.276 MeV. The experimental distribution shows a characteristic deep minimum, due to destructive interference, which is partially filled in due to finite target thickness effects (see Sec. III C 3). A surface fit utilizing the *R*-matrix methods described below (for extensive discussion, see Sec. III C 3) indicates the depth that the interference minimum should have for a zero thickness target. The Legendre fit [Eq. (3)] also shown in the figure, however, closely matches the interference minimum even though no target thickness effect has been taken into account, demonstrating how Legendre fits can incorrectly compensate for a finite target thickness. Surface fits for target thicknesses of $\Delta=0$ and $\Delta=100$ keV, quoted in Ref. [13], are shown[8] in Fig. 1.

3. Error determination

As in Ref. [12] we find that most of the data investigated show the presence of systematic errors and inconsistencies with respect to one another as well as strong correlations of parameters. Furthermore, the quantities $S_{E1}(300)$ and $S_{E2}(300)$ are not direct parameters of either the *R*- or *K*-matrix theory, even though we try to approach this as much as possible (Sec. III.A.2.). This poses the immediate problem of the error determination in a statistical analysis with obvious systematic contributions, high parameter correlation, and derived secondary quantities, to which there can be no exact solution. As in Ref. [12] we therefore take (intuitively) as an acceptable range of parameters $\chi^2_{\rm limit}=\chi^2_{\rm min}+9\chi^2_\nu$, with χ^2_ν being the error per point of the combined fits. In our simulations, where no systematic errors are present, we also used Monte Carlo methods, i.e., multirandomization and analysis of the resulting distributions, to estimate our errors. Such Monte Carlo methods would have led to the most appropriate error determinations if all measurements fitted had been free of systematic error.

C. Results from *R*- and *K*-matrix fits

In the following sections we will use several methods for incorporating the published radiative capture and elastic scattering angular distributions into the *R*- and *K*-matrix analyses.

[8]Throughout the paper elastic scattering target thicknesses are quoted for an α laboratory energy of 1 MeV. In the integrations over the target thickness, the energy dependence of the stopping power was, however, included.

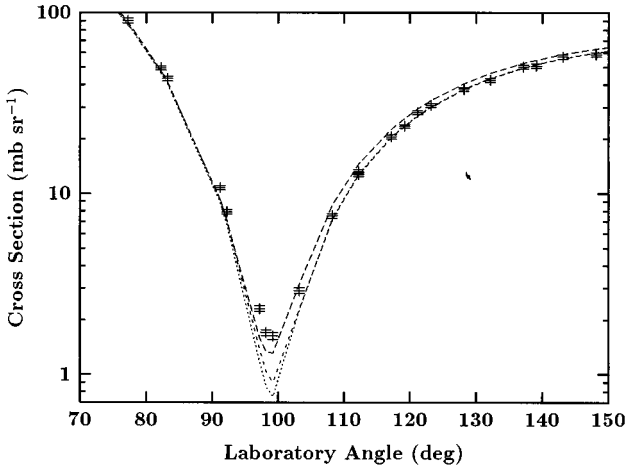

FIG. 1. Experimental angular distribution for E_α=3.276 MeV [13] and the Legendre fit (long dashes) corresponding to Eq. (3). *R*-matrix surface fits for $\Delta=0$ (dotted curve) and 100 keV (short dashes) target thicknesses are also shown.

First, in Sec. III C 1, we will assume that σ_{E1} is sufficiently well determined by the ^{16}N experiments [12] so that the $E1$ and $E2$ contributions to the ^{12}C$(\alpha,\gamma)^{16}$O reaction can be reasonably well determined (including the correct propagation of errors) from the measured σ_{E1}/σ_{E2} ratios that have been determined from the analyses of γ-ray angular distributions at various energies [7,9,11]. Such a procedure should result in improved sets of both $E1$ and $E2$ cross sections, which can then be incorporated into the parametrizations for extrapolation of the total *S* factor to 300 keV. Similar approaches have been published previously, e.g., [9,11,23]. However, these earlier $E2$ data sets were clearly affected by the poorly known $E1$ component.

In a second approach (Sec. III C 2) we use the method of surface fits for the first time to analyze the γ-ray angular distributions directly in terms of the *R*- and *K*-matrix parametrizations, while still retaining the analysis of the elastic scattering in terms of the phase shifts [13] and the results of the β-delayed α spectrum from the ^{16}N-decay experiments in the simultaneous analysis.

Finally, a full surface analysis of both the γ-ray and elastic scattering angular distributions, in conjunction with the ^{16}N-decay results of [12], is presented in Sec. III C 3 in terms of an *R*-matrix analysis.

1. K-matrix fits to E2 data derived from best published E1 values

New values for the σ_{E2} cross sections were determined employing the best set of σ_{E1} values from Ref. [12] in conjunction with the ratios σ_{E2}/σ_{E1} from Refs. [7,9,11]. These are shown in Fig. 2.

The σ_{E2} cross sections and the $\ell=2$ phase-shift data of Ref. [13] were then analyzed in terms of the *K*-matrix parametrization described in Sec. III A 2. The calculated values for χ^2_ν for fixed values of $S_{E2}(300)$ over the range 0–160 keV b, each time allowing five parameters to vary (the γ width of the subthreshold state was fixed to its experimental value and the position of the echo pole was fixed at 8 MeV [23]), are shown in Fig. 3.

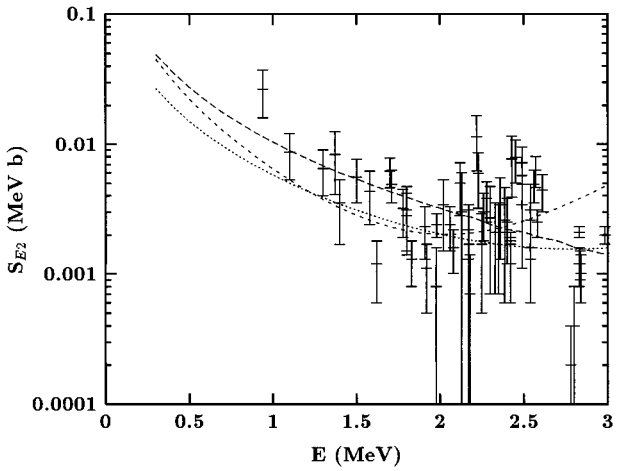

FIG. 2. S_{E2} values derived from the data of Refs. [9,11] as described in the text. The short-dashed and dotted curves show the K-matrix best fits to the individual S_{E2} values derived from Ref. [11] and Ref. [9] data, respectively. The microscopic potential model prediction of Ref. [9] is shown by the long-dashed curve.

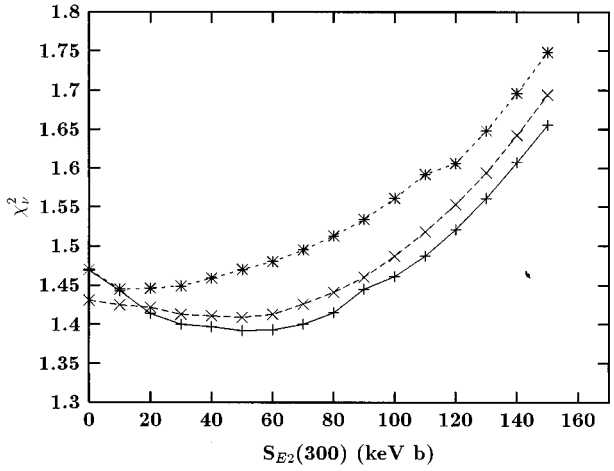

FIG. 4. Dependence of χ^2 on $S_{E2}(300)$ for $S_{E1}(300)$ equal to 70 keV b (solid curve), 80 keV b (long dashes), and 90 keV b (short dashes) calculated from surface K-matrix fits to the data of Ref. [11].

Best K-matrix fits for Refs. [9] and [11] to the capture data are shown in Fig. 2. To test the dependence of the results on the choice of background parametrization, we have performed other K-matrix fits to the data, in which the position of the echo pole was allowed to vary. In all of the K-matrix analyses, we find that the present data do not constrain the value of $S_{E2}(300)$ to an astrophysically useful level of precision.

The same conclusion was reached in our two-level R-matrix fits. Again we observe that χ^2_ν (the quality of the fits) is nearly constant for values of $S_{E2}(300)$ over the range 0–150 keV b.

2. Surface fits to radiative capture data

In this section, we describe an analysis which, for the first time, utilizes R- and K-matrix surface fits to the combined set of radiative capture angular distributions described in Sec. III B 1, along with the usual analyses of the $\ell=1$ and $\ell=2$ elastic scattering phase-shifts [13], and the ^{16}N-decay data [12]. In these fits we have chosen to use the phase shift data of Ref. [13] with their larger errors rather than our own recalculated values. The R-matrix formalism for the $E2$ part of the radiative capture is described in Sec. III A 1. For the K-matrix studies the $E1$ parametrization is described in [12], while the $E2$ parametrization was chosen as outlined above (Sec. III A 2). The states used for each partial wave are specified in Sec. III A.

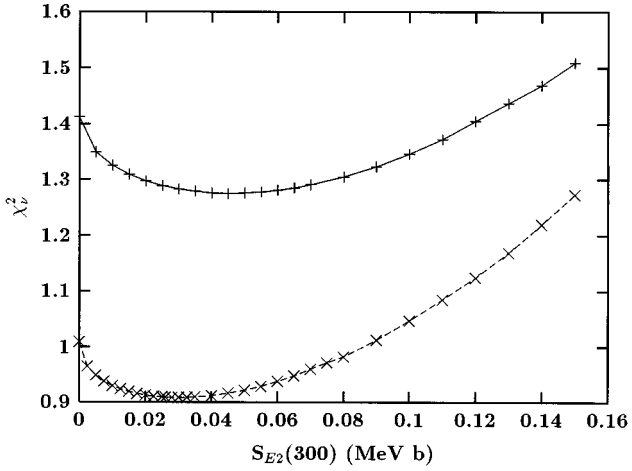

FIG. 3. χ^2 dependence on $S_{E2}(300)$ as calculated in K-matrix fits to the individual S_{E2} values derived from the data of Refs. [11] (dashed curve) and [9] (solid curve). The curves are simply guides to the eye.

We have performed a series of K-matrix fits for various fixed values of $S_{E1}(300)$, varying $S_{E2}(300)$ between 0 and 150 keV b. The values of χ^2_ν obtained in these fits are shown in Fig. 4, for the angular distributions of Ref. [11]. Again we find that the data do not permit astrophysically meaningful constraints on $S_{E2}(300)$. The same conclusion was reached when fitting the angular distributions of Ref. [9].

For the R-matrix calculations in this section, the radius parameter was fixed at $a=6.5$ fm, the best value from Ref. [12]. Fig. 5 shows a contour plot of χ^2 as a function of $S_{E1}(300)$ and $S_{E2}(300)$. It is apparent from the figure that $S_{E1}(300)$ and $S_{E2}(300)$ in this combination of fitted data sets are nearly linearly independent; i.e., the variation of one of them does not, in general, substantially influence the result obtained for the other variable. An interesting feature of Fig. 5 is that destructive interference in the $E1$-radiative-capture channel in the energy region between the 7.1 and 9.6 MeV states is excluded, confirming the conclusion reported previously in Ref. [12]. The minimum of the χ^2 distributions is found at $S_{E1}(300)=80.8$ keV b and $S_{E2}(300)=11.4$ keV b, demonstrating the strong dependences on $S_{E1}(300)$ on the ^{16}N-decay data and $S_{E2}(300)$ on the elastic scattering data.

An important result following from the analysis of the elastic phase-shift data of [13] is that, in all our R- and K-matrix studies to date, including those reported in [12], the analysis of the elastic data *without* the inclusion of the ^{16}N results invariably led to a minimization where the reduced α widths of both the $J^\pi=1^-$ and $J^\pi=2^+$ subthreshold states were close to zero. This result for the $J^\pi=1^-$ subthreshold

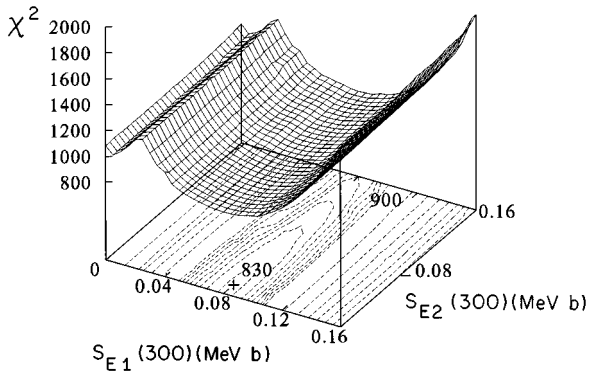

FIG. 5. Contour plot of χ^2 versus $S_{E1}(300)$ and $S_{E2}(300)$ for $a=6.5$ fm, calculated using the elastic phase-shift analysis of Ref. [13] and the other data as discussed in the text. Contour lines proceed in steps of 10 from $\chi^2=830$ to 900, and in steps of 100 from 900 to 1600. The minimum of the fit is marked with a cross. The best values are $S_{E1}(300)=80.8$ keV b and $S_{E2}(300)=11.4$ keV b.

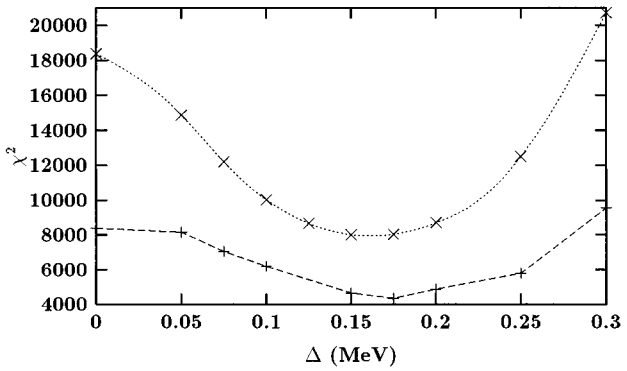

FIG. 6. Dependence of the least squares fit parameter χ^2 on the target thickness is shown for both the R-matrix analysis with $a=6.5$ fm (dashed curve) and the K-matrix analysis (dotted curve) for the angular distributions of [13]. For the R-matrix fits the angular distributions at $E_\alpha=3.571$, 4.251, 5.251, and 6.558 MeV were excluded.

state is clearly in contradiction to that reported in [12], while the latter is in disagreement with the α-transfer data (see Sec. V C). Whenever the ^{16}N results are included, however, the simultaneous analysis consistently leads to a finite value of the reduced α width of the $J^\pi=1^-$ state and to a value of $S_{E1}(300)$ near 80 keV b. This behavior is discussed further in the next section.

3. Full surface fits to elastic scattering and radiative capture data

Here, the results of performing surface fits to the angular distributions of both the radiative capture data and the elastic scattering data are presented. Although the β-delayed α spectrum of ^{16}N was included, as usual, in most of the fits, it was excluded in the calculations for one contour plot in order to emphasize certain aspects of fits to the elastic scattering data. For the reasons given above these analyses were performed for the R-matrix fits only.

We begin by reporting the results of some studies specifically related to the analysis of the elastic scattering distributions. First, the effects of the target thickness were taken into account for the fits to the elastic data. This was done initially by integrating over the appropriate energy-dependent target thickness when calculating the theoretical yield for each data point in each iteration of the least squares minimization routine. However, in order to avoid the extensive computation necessary for a full integration of this type in the numerous fits for the contour plots, an approximation was used. A correction matrix was produced where the element for each data point was taken to be the ratio between the best-fit theoretical value with a full integration and the corresponding value calculated with the same R-matrix parameters but no integration. Thus, in these later minimizations, the theoretical value at each point was multiplied by the corresponding ratio of the correction matrix to approximate the integration. Many subsequent comparisons have shown that the results for the two methods are essentially the same.

In Ref. [13], ^{12}C target thicknesses of 17–34 μg/cm^2 are reported which correspond to energy losses Δ of about 34–74 keV at $E_\alpha=1$ MeV. The target plane was inclined at 30° relative to the beam axis, resulting in a doubling of this thickness. We have performed a series of R- and K-matrix surface fits for a range of energy-dependent target thicknesses. The best R-matrix fit (for $a=6.5$ fm) was found, however, for $\Delta=175$ keV as shown in Fig. 6. The inclusion or exclusion of distributions at narrow resonances, largely responsible for large values of χ^2, does not substantially affect this result. However, in a further series of calculations concerning target thickness effects (which we do not report here in detail) it has been found that the best value for the target thickness is independent of the value of the interaction radius a. Because the best-fit value at the minimum in χ^2 is outside the quoted range of target thicknesses, and because other unidentified processes may have contributed to these effects, we chose an average target thickness of $\Delta=100$ keV, close to the center of the quoted thickness range in Ref. [13], for the subsequent calculations. We note that the small value of the subthreshold reduced width amplitudes (see below) is not strongly affected by any reasonable choice of value of the target thickness Δ.

Regarding the dependence of the least squares fit on the interaction radius a, we note that the best fits to the elastic distributions alone are achieved for the unusually low radius of $a=4.5$ fm.

Fits to the elastic data posed many additional difficulties, particularly associated with energy-dependent systematic errors. This was already noted in Ref. [13] where several of the derived phase shifts were excluded because they occurred at very sharp resonances. In order to get reasonable values for the total χ^2 in our work, several angular distributions near sharp resonances were excluded from the surface fits. Even so, with this exclusion and the target thickness correction, values for the χ^2/point of 2.5→3.5 were obtained for the best fits. In Fig. 7 the normalized deviations of the experimental values from the corresponding theoretical fits are shown for the high-energy data points in the distributions. Data points are shown in a linear order on the x axis by ascending angle and energy. Clearly, systematic and periodic deviations between fit and data for each individual distribution are visible. As noted in the previous section where the elastic phase-shift data were used, the surface fits to the elas-

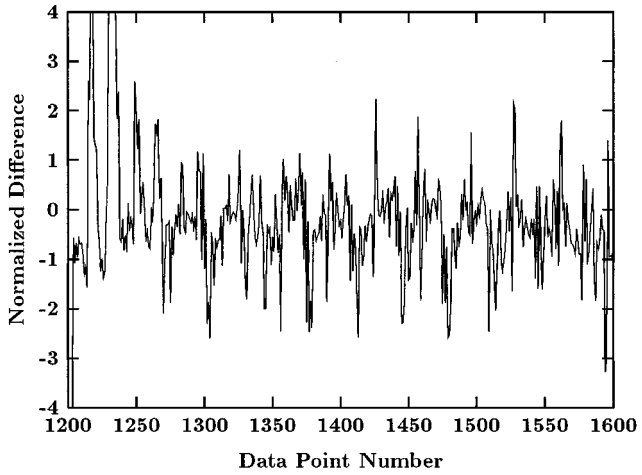

FIG. 7. Normalized differences (experimental value minus fitted value divided by the error), calculated with surface R-matrix fits to some of the higher-energy ($E_\alpha > 5.8$ MeV) angular distributions of Ref. [13] are shown as a function of the data point number, i.e., data points ordered by angle and energies. Each of the periodic patterns corresponds to an angular distribution at one energy. These patterns indicate repetitive systematic problems.

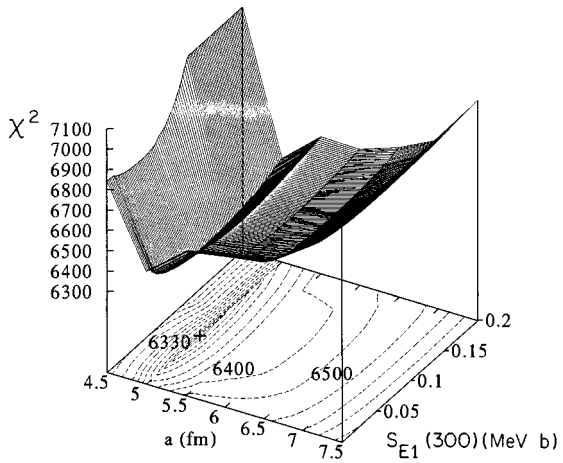

FIG. 8. Dependence of the least squares parameter χ^2 on $S_{E1}(300)$ and the interaction radius a for a ^{12}C target thickness of 100 keV. The minimum of the R-matrix surface fit is marked with a cross. The β-delayed α spectrum of ^{16}N [12] was not included in the fits for this figure. Fits with χ^2 exceeding 7100 were set to this value and not explored further.

tic angular distributions also lead to very small values for the reduced α widths of the $J^\pi = 1^-$ and 2^+ subthreshold states. In addition, the width of the 6.131 MeV $J^\pi = 3^-$ was found to be significantly larger than that reported in [12]. These results are discussed in more detail in the following.

The results of the minimization of the p- and d-wave fits, which yielded small values for γ_{11} and γ_{12} both for fits to the phase shifts and for surface fits to the data of Ref. [13], are in contradiction to the results reported in Ref. [13] in which rather large values of the reduced α width of both the $\ell = 1$ and $\ell = 2$ subthreshold states were found. However, the authors of Ref. [13] restrict their $\ell = 2$ background state energy to be above $E_{32} = 15$ MeV using arguments about the position of physical states.[9] The authors of Ref. [13] find, however, their best fit for the lowest of their background state energies and the smallest reduced width (Table 4 of [13]). Lowering the background state energy further would have led to the (close to) zero result we find.

In the next phase of this study the analysis was expanded to full surface fits to both the radiative capture and the elastic scattering angular distributions, with emphasis at this stage only on the $E1$ component of the radiative capture. For these R-matrix fits, the influence of the choice of the interaction radius a was explored in detail. However, in order to highlight the effects of the elastic scattering angular distributions in the determination of the reduced α widths of the subthreshold states, the analysis was done without the inclusion of the β-delayed α spectrum of ^{16}N. Figure 8 shows a contour plot for χ^2 as a function of $S_{E1}(300)$ and the interaction radius a, for a target thickness Δ of 100 keV. The fit is strongly dominated by the a dependence of the elastic scattering. At the minimum for χ^2 the value of the interaction radius was $a = 5.0$ fm and $S_{E1}(300)$ was found to be 70 keV b, ranging from 30 to 165 keV b. This value of $S_{E1}(300)$ is a compromise between the radiative capture data tending to high values and the elastic scattering data leading to low values. This figure should be compared with Fig. 16 of Ref. [12] where a similar plot is shown that employs, however, the phase-shift results of Ref. [13] and the ^{16}N data of [12]. The results of the two figures are in contradiction with respect to the strong a dependence found with the inclusion of the full elastic scattering data set.

The analysis was then further broadened to include the β-delayed α spectrum of ^{16}N, with emphasis now on both the $E1$ and $E2$ components of the radiative capture. Figure 9 shows a contour plot for χ^2 versus $S_{E2}(300)$ and the interaction radius a. For these fits, also, a target thickness of $\Delta = 100$ keV was used. At the minimum of χ^2, best-fit values were found to be $S_{E2}(300) = 13$ keV b and $a = 5.5$ fm. With the error criterion in Sec. III B 3 for χ^2, Fig. 9 leads to the restrictions $S_{E2}(300) \leqslant 35$ keV b and, for the interaction radius, $5.2 \leqslant a \leqslant 6.0$ fm. This range for a is significantly lower than that found in the analysis of [12] where the best value was found to be 6.5 fm. The value of a at the minimum is increased relative to the fits of Fig. 8 because of the influence of the ^{16}N α spectrum. The relatively low values for $S_{E2}(300)$ at the minimum of χ^2 are attributed solely to the effects of the elastic angular distribution data. Also, the restrictions on $S_{E2}(300)$ for small interaction radii a are stronger than for larger a. For the case where $a = 4.5$ fm, the χ^2 minimum is obtained with destructive interference between the direct capture and the subthreshold pole term for the radiative capture channel, and yields a value of $S_{E2}(300) = 1$ keV b, while the minimum for constructive interference is found at 30 keV b. As can be seen by comparison with Fig. 5, the restrictions on $S_{E2}(300)$ are far more stringent for any interaction radius a than those imposed by the phase-shift data as, for example, in the analyses of Sec. III C 1 and III C 2. The minimum of χ^2 is found for $S_{E1}(300)$ at 82 keV b.

[9] We find the best values for $E_{32} \leqslant 10$ MeV.

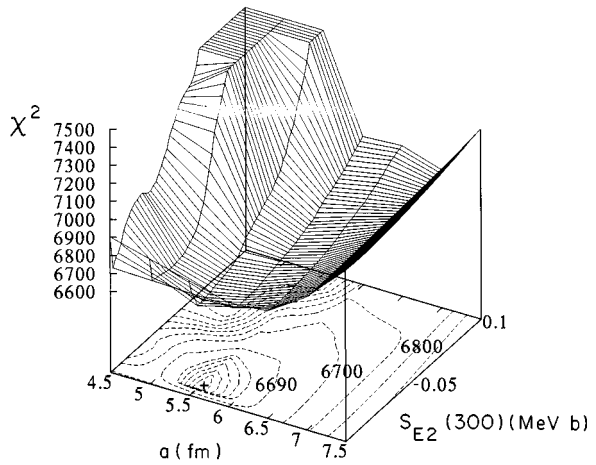

FIG. 9. Dependence of the least squares parameter χ^2 on $S_{E2}(300)$ and the interaction radius a for a ^{12}C target thickness of 100 keV at 1 MeV. The minimum of the R-matrix fit is marked with a cross. Fits with χ^2 exceeding 7500 are set to this value and not further explored. The best fit leads to values of $S_{E2}(300) \leqslant 35$ keV b and $5.2 \leqslant a \leqslant 6.0$ fm.

The large value for the reduced α width of the $J^\pi = 3^-$ subthreshold state derived here is at variance with the analysis of the β-delayed α spectrum of ^{16}N reported in [12]. In that study, β feeding to the subthreshold state (6.130 MeV) only was allowed, whereas in the present study a considerable improvement in the fits was achieved when the β-feeding factors of both the 11.4 MeV and the background state were allowed to be variable parameters. The reason for this improvement is that the elastic scattering data try to force an excessive subthreshold 3^- α width into the ^{16}N spectrum which can only be compensated for by including additional states into the fit to the β-delayed α spectrum of ^{16}N. As a consequence, more structured f waves and a larger variation of $S_{E1}(300)$ with the interaction radius a are produced.

In Figs. 10(a)–10(h) we show, representing all data sets, some of our best R-matrix surface fits to the γ-ray angular distributions, elastic angular distributions (with $\Delta = 100$ keV target thickness corrections), and the β-delayed α spectrum of ^{16}N obtained by using R-matrix theory.

In Table II the least squares contributions for the best fit taking all available primary data into account are shown.

4. Conclusions drawn from the fits to the experimental data

In the fits using the published phase shifts of [13], $S_{E2}(300)$ was poorly constrained. To understand the origin of the uncertainty in $S_{E2}(300)$, we note that the value of $S_{E2}(300)$ is dominated by the reduced α width of the subthreshold 2^+ state. However, in the energy regime over which present data exist ($E \geqslant 1$ MeV), the high-energy wing of the bound state interferes with the undetermined background (tails of higher-lying resonances and the DC component). Since neither the full nature of the background nor the extent of the interference is known, the data can be fitted over a large range of values of the reduced α width of the subthreshold state, leading to the observed uncertainty in $S_{E2}(300)$ in our fits. Thus we find that, with the published phase shift data, all values of $S_{E2}(300)$ below 140 keV b are acceptable with the error criterion of Sec. III B 3 (Fig. 5 of Sec. III C 2).

We have found, however, that the analysis involving surface fits to the elastic scattering angular distribution data imposed more stringent restrictions for each partial wave than those found from the phase-shift analysis described above. It was found that these restrictions were not important for the $E1$-radiative-capture results as long as the ^{16}N α spectrum was fitted simultaneously. However, they were dominant for the $E2$ component. The results for the $\ell = 1$ and $\ell = 3$ fits are hard to reconcile with fits to the β-delayed α spectrum of ^{16}N. For the $E2$ radiative capture, significantly smaller results are found for $S_{E2}(300)$, pointing to a very small reduced width for the subthreshold 2^+ state in contradiction to the results of α-transfer reactions and theoretical predictions (see Sec. V). Because of these concerns, and the questions raised previously about both the magnitude of the statistical errors and the presence of significant systematic errors in the elastic scattering data (at the extremely low level pertinent to the subthreshold states; see Sec. IV B), we are not prepared to adopt the tighter restrictions deduced from our surface fits. We conclude that our present analysis leads to the following results: For the $E1$ component the result from Ref. [12] still remains the most solid determination and is $S_{E1}(300) = 79 \pm 21$ keV b. For the $S_{E2}(300)$ component, the best estimate from the present analyses is $S_{E2}(300) \leqslant 140$ keV b, as quoted above.

IV. POSSIBLE RESTRICTIONS ON $S(300)$ BY IMPROVED DATA

In this section we explore what possible constraints could be imposed on the rate of the $^{12}C(\alpha,\gamma)^{16}O$ reaction at the astrophysically most important energy if improved data were available, and where such improvements are most likely to come from. To do this, we first simulate possible experiments by randomizing likely cross sections and angular distributions. These pseudodata are then subjected to many of the kinds of R- and K-matrix analyses described above to determine what the possible error limits may be. Since it is difficult to simulate in any realistic way the systematic errors which may afflict future experiments, our predictions are based solely on statistical uncertainties. In this connection, it is important to note that the error criterion defined in Sec. III B 3 is inappropriate for error determination in these simulations. In fact, for a purely statistical analysis (i.e., with no systematic errors) as in the discussion below, that criterion would correspond to a 3σ error, if the fitting formalism were linear in its parameters and the S factor a parameter of the fit.

A. Possible limits imposed by radiative capture data

Because the actual set up of future experiments designed to measure directly the capture rate of $^{12}C(\alpha,\gamma)^{16}O$ is subject to much uncertainty, we make the following assumptions about the parameters of a possible experiment. First, we have assumed that a 4π γ-ray detection geometry will be available and that the analysis will involve fits to the total cross section of $^{12}C(\alpha,\gamma)^{16}O$, i.e., the sum of the cross sections of the radiative $E1$ and $E2$ ground state transition. Second, we

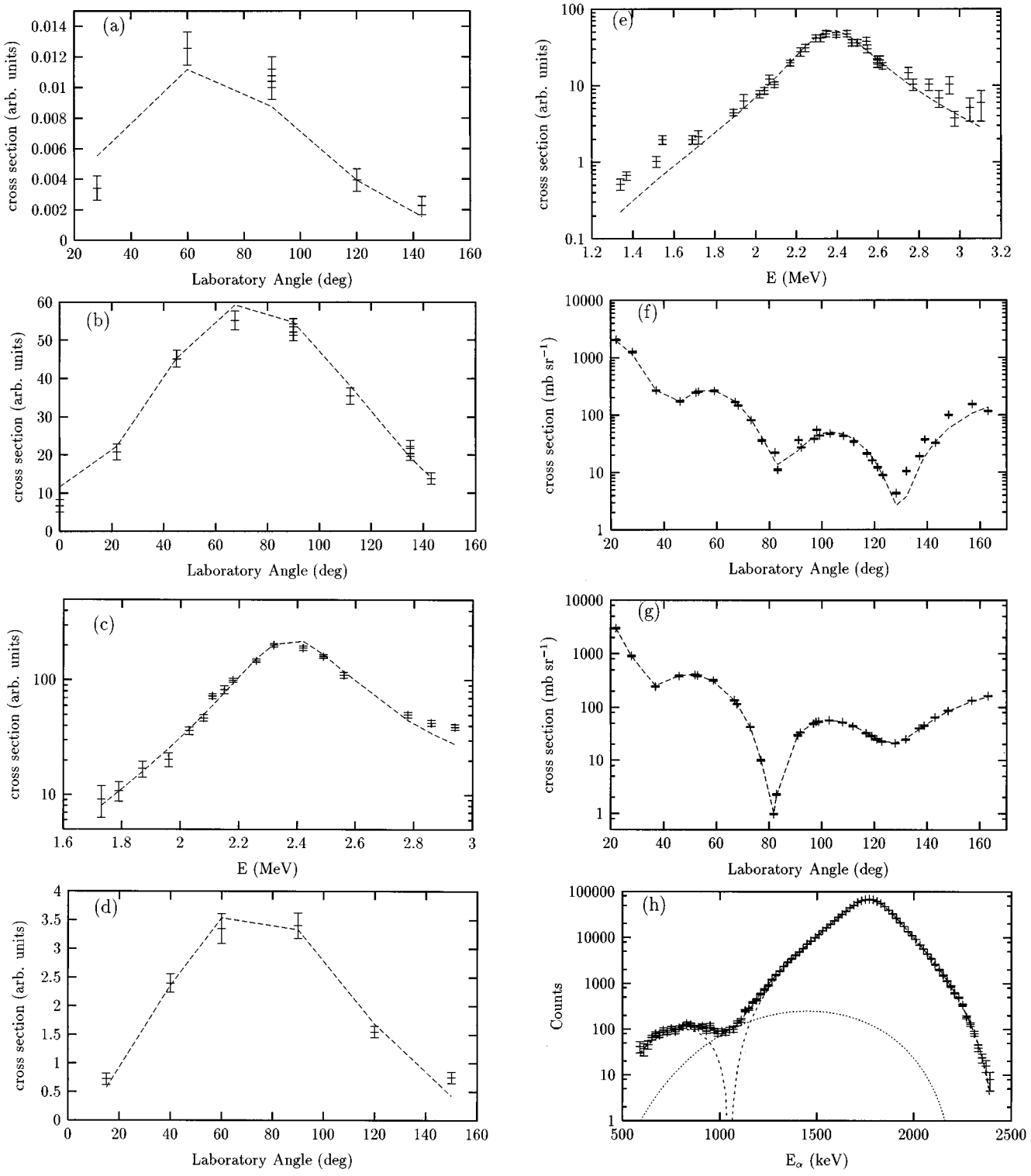

FIG. 10. Results of the best R-matrix surface fits (with a =5.5 fm) to some representative radiative capture angular distributions, the elastic angular distributions (with Δ=100 keV), and the ^{16}N data. Shown are the γ-ray angular distributions of (a) Ref. [11] at E_α=2.571 MeV, (b) the γ-ray angular distribution of Ref. [7] at E_α=2.420 MeV, (c) the 90° data of Ref. [7], (d) the γ-ray distribution of Ref. [9] at E_α=2.360 MeV, (e) the γ 90° measurement Ref. [8], the elastic α-particle angular distributions of Ref. [13] at (f) E_α=5.919 MeV and (g) E$_\alpha$=6.458 MeV, and (h) the β-delayed α spectrum of ^{16}N [12].

assume (probably over-optimistically) that the energy range of the measurements goes down to E=500 keV and that, above E=1 MeV, the energies of existing measurements will be used. Finally, we have chosen to attribute 20% statistical error to data points with less than 0.1 nb cross section, 15% for points between 0.1 and 1 nb, 10% for points between 1 and 10 nb, and 5% for points above 10 nb to simulate to a degree real experimental conditions. The existence of such experimental data would indeed represent a very considerable improvement over any data presently available.

TABLE II. Contributions to χ^2 for a best fit with a ^{12}C target thickness of 100 keV and $a=5.5$ fm.

Fit to	Number of points	Total χ^2
γ [11]	96	258
γ [7]	40	120
γ [7] 90°	17	77
γ [9]	18	30
γ [8]	36	110
^{16}N [12]	87	100
elastic [13]	1583	5926

Arbitrarily we have selected a previous solution with 79 keV b for the $E1$ component and 70 keV b for the $E2$ component, i.e., $S(300)=149$ keV b, as the reference cross sections to be randomized. In addition, the ^{16}N data of Ref. [12] were included in the subsequent fits. Elastic data were excluded on the basis of the systematic problems noted above. Fits were done only for $a=5.5$ fm as the original reference cross sections were calculated at this interaction radius. A number of sets of pseudodata were derived from the reference cross sections, and each was analyzed with the R-matrix procedure. These fits showed that although each minimization did not necessarily yield the reference value for $S(300)$, a series of such randomizations produced a statistical distribution whose center was close to the reference value and whose width is indicative of the likely restrictions on the total S factor. The widths σ of these distributions are 2.2, 20.1, and 20.1 keV b for the $E1$, $E2$, and total S factors, respectively, as shown in Fig. 11.[10] We would therefore expect relative errors for the total S factor of about 13% for the particular conditions of these randomizations for a 1σ error in the Monte Carlo simulations.

To compare the restrictions on $S(300)$ based on the methods of the previous sections an arbitrary pseudodata set was selected for detailed analysis of parameter correlations. Figure 12 shows an example of such a radiative capture pseudodata set and fits to these data. The value of χ^2 was then calculated for this pseudodata set as a function of $S_{E2}(300)$ with $S_{E1}(300)$ constant at the value noted above resulting in the usual least squares parabola.[11] The error based on our error criterion (Sec. III B 3) for this one distribution is about 40 keV b, which is twice that of the Monte Carlo simulation. Further simulations show that the absolute errors stay nearly constant for most values of $S_{E2}(300)$; i.e., the relative error decreases with $S(300)$.

As a result of this and other simulations, it appears that it will be difficult in the near future to obtain the astrophysically desired precision for the helium-burning problem through improvements in the γ-ray experiments alone if the statistical accuracy stays close to the level of the present experiments. Either measurements down to about $E=500$ keV with considerable statistical accuracy or measurements of higher energies with many-times improved accuracy will be required to approach the precision required by stellar models (about 30%), as additional simulations have demonstrated.

B. Possible limits imposed by improved elastic scattering data

In previous sections we have seen that the elastic angular distributions of Ref. [13] indeed pose considerable restrictions on $S_{E2}(300)$ (see Fig. 9) which would lower the uncertainty in $S_{E2}(300)$, if those data did not have systematic problems as discussed above. For this reason, we have created elastic pseudodata by randomizing a previous R-matrix fit to the elastic scattering angular distributions of Ref. [13] to gain further insight into how far improved elastic scattering data could restrict $S_{E2}(300)$. For convenience, the same energies and angles as those of Ref. [13] were taken. In the randomization procedure, we have used a statistical error of 1.5%, equivalent to the rough average of statistical errors in Ref. [13], and an error of 1% in another simulation. Using the pseudodata set corresponding to the 1.5% randomization, we have then explored the dependence of χ^2 on γ_{12} with the p-wave parameters either fixed or as free variables. Neither the β-delayed α spectrum of ^{16}N nor the radiative capture data were used in these initial fits. For computing time reasons some of the calculations were performed for zero target thickness as we do not find any change in statistical behavior and only minor changes in the parameters. Target thicknesses were included in some of the simulations because the base fits, being randomized, were derived from fits to the data of [13] using finite target thicknesses. No noticeable effects were noticed from inclusion or exclusion of the target thickness. The results are shown in Fig. 13.

If the p-wave parameters are left free in these fits, the reduced width amplitude γ_{11} closely follows γ_{12}. This again

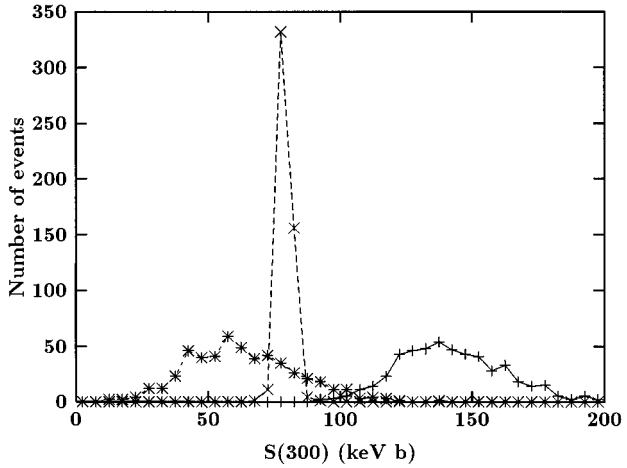

FIG. 11. The $S_{E1}(300)$ (crosses), $S_{E2}(300)$ (stars), and $S(300)$ (plus signs) distributions from 505 R-matrix fits to the randomized $^{12}C(\alpha,\gamma)^{16}O$ total cross section pseudodata as described in the text. The ^{16}N data of Ref. [12] were included in the fits, whereas the elastic data of Ref. [13] were not.

[10]Note that the $E1$ and the $E2$ distributions are not statistically independent here; i.e., the distribution widths do not add necessarily in quadrature for the total cross section distribution. This is largely due to the higher statistical weight of the radiative capture (pseudo)data (fitted as the total sum) compared to the ^{16}N data, while in the results shown in Fig. 5 the $\ell=1$ part was statistically entirely fixed by the β-delayed α decay of ^{16}N with little weight coming from the radiative capture data.

[11]Thus $S(300)$ varies as $S_{E2}(300)$.

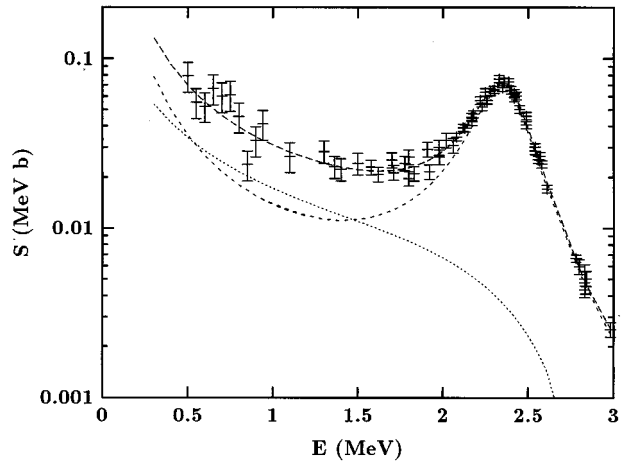

FIG. 12. Best fit, including $E1$ (short dashes), $E2$ (dots), and total S factor (long dashes), to a randomized radiative capture distribution (''pseudodata'') as discussed in the text.

demonstrates how closely some of the parameters are correlated. We also note that the constraints on γ_{12} become tighter for decreasing interaction radii a.

Simultaneous fits employing the elastic pseudodata, the β-delayed α spectrum of ^{16}N, and the radiative capture data [7–9,11] were then carried out and the results of this study are shown in Fig. 14. Values of $a=6.5$ and 6.0 fm for the radius parameter and target thicknesses of $\Delta=0$ and 100 keV were used. With our error criterion, the χ^2 distributions of Fig. 14 result in errors on $S_{E2}(300)$ of 10 keV b (1.5%) and 7 keV b (1%) , respectively, to which additional experimental systematic errors and some variations arising from the a dependence of the data would have to be added in the fits to real data. For this particular randomization our error criterion corresponds to 3 times the Monte Carlo error discussed in the next paragraph.

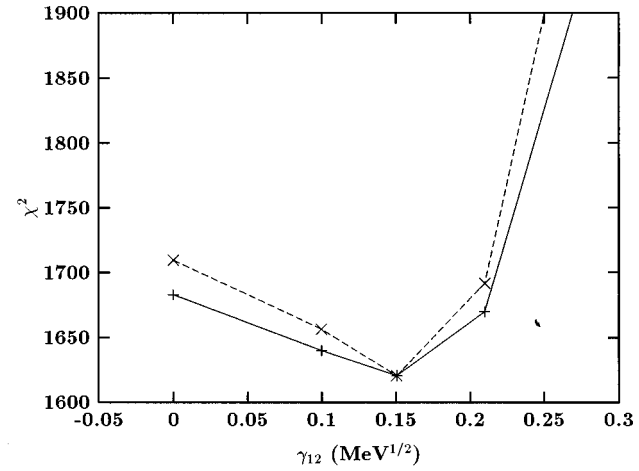

FIG. 13. R-matrix analysis (with $a=6.5$ fm and zero target thickness) of the randomized elastic scattering angular distribution pseudodata with 1.5% statistics. The dependence of χ^2 on γ_{12} for all parameters allowed us to vary (solid curve) and the p-wave parameters fixed (dashed curve) are shown.

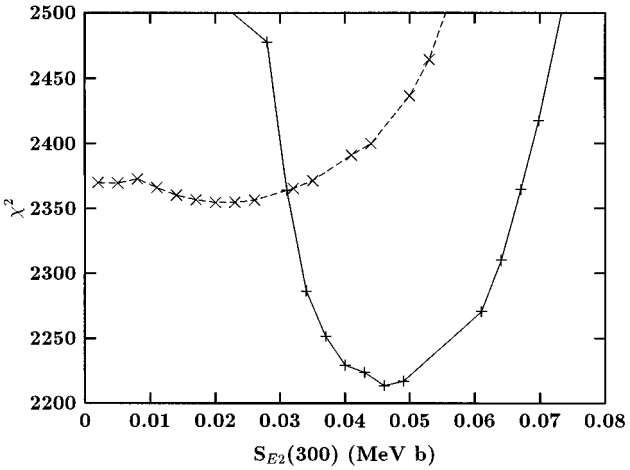

FIG. 14. χ^2 versus $S_{E2}(300)$ for an R-matrix analysis of the randomized elastic scattering angular distribution pseudodata calculated for 1.5% statistics (dashed curve with $a=6.5$ fm and zero target thickness) and 1% statistics (solid curve with $a=6.0$ fm and 100 keV target thickness). The β-delayed α spectrum of ^{16}N and the experimental radiative capture angular distribution data were included in both analyses. The different depths of the minima as well as the different widths of the distributions are to a considerable degree caused by the different interaction radii a.

Alternatively, we have performed Monte Carlo simulations to determine the effectiveness of elastic angular distributions in restricting the value of $S(300)$. First, a reference set of elastic angular distributions was created as described above but with $S_{E2}(300)=50$ keV b, i.e., $S(300)=130$ keV b. The reference angular distributions were then randomized to create a set of pseudo elastic angular distributions which were then included in a simultaneous R-matrix analysis, along with the experimental radiative capture and ^{16}N data to yield fitted values for $S_{E1}(300)$, $S_{E2}(300)$, and $S(300)$. This randomization and fitting procedure was then repeated several times to give distributions for the values of these quantities. Three sets of Monte Carlo simulations were done for statistical fluctuations of 1%, 2%, and 5%, respectively in the randomization procedure. The distributions are similar to those in Fig. 11 and result in 1σ errors for $S(300)$ of 2.2, 6.4, and 11.3 keV b, respectively, for these levels of statistics, with similar errors for $S_{E2}(300)$ and errors less than 1.5 keV b for $S_{E1}(300)$. It may be noted that the Monte Carlo simulations indeed show that the statistical level achieved in Ref. [13] is sufficient to constrain the total S factor of $^{12}C(\alpha,\gamma)^{16}O$ to a precision of 3% for this randomization.

The influence of the $\ell=1$ and $\ell=2$ subthreshold states on the elastic scattering distributions is, indeed, relatively subtle. To demonstrate this and to estimate the effects which can be expected in any elastic α-scattering experiment, we have created a set of pseudodata from an R-matrix fit ($a=6.5$ fm) to the angular distributions of Ref. [13]. Figures 15 and 16 show the absolute and relative differences, respectively, for the $\ell=2$ phase shift calculated with values of $\gamma_{12}=0$ and 0.2 MeV$^{1/2}$. Similar results are found for comparable variations of γ_{11}. The phase shifts used in Figs. 15,16 were obtained from a least squares minimization fit to

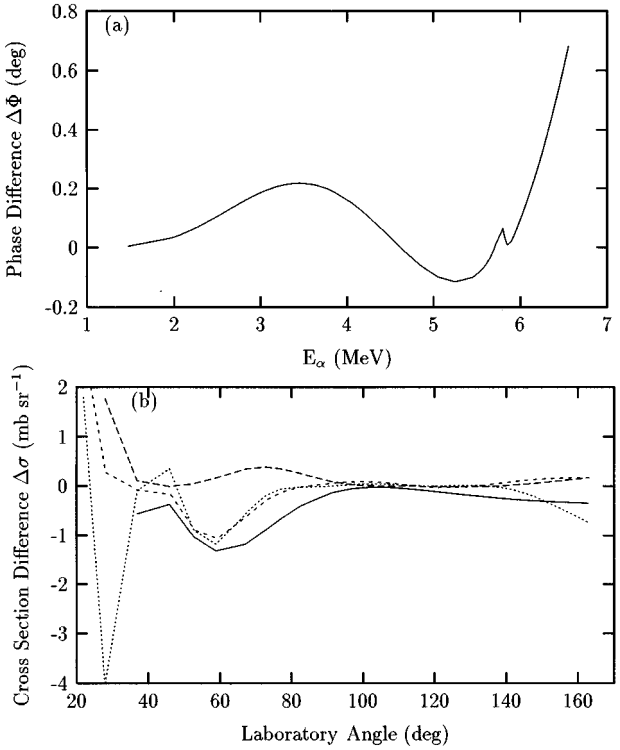

FIG. 15. (a) Absolute $\ell=2$ phase-shift differences between two R-matrix surface fits (both with $a=6.5$ fm) to the elastic scattering angular distribution pseudodata (with 1.5% statistics), first with the amplitude γ_{12} fixed at 0 and then with γ_{12} fixed at 0.2 MeV$^{1/2}$. (b) Absolute differences in cross sections from an R-matrix analysis of the elastic scattering angular distribution pseudodata at the four energies $E_\alpha=3451$, 5251, 5819, and 6258 keV (solid, short-dashed, long-dashed, and dotted curves, respectively) for the same conditions as in (a).

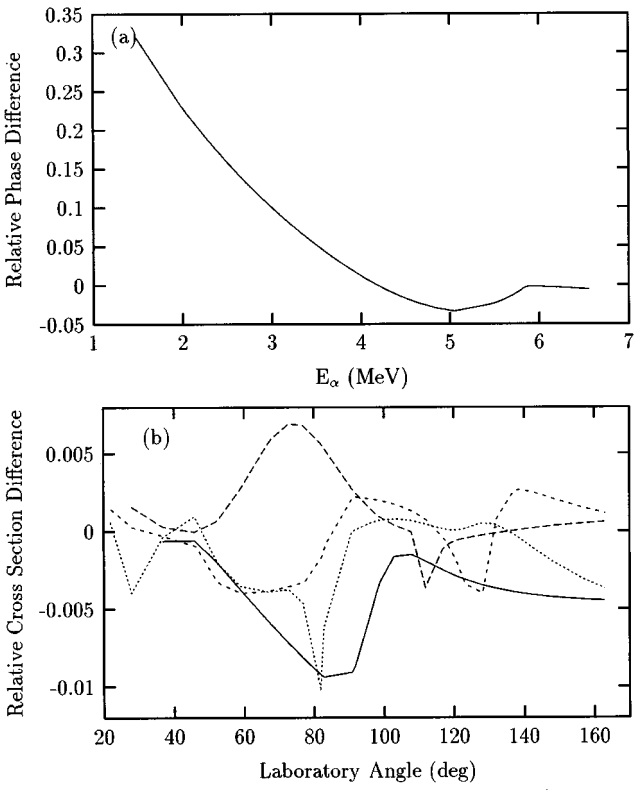

FIG. 16. (a) Relative $\ell=2$ phase-shift differences between two R-matrix surface fits (both with $a=6.5$ fm) to the elastic scattering angular distribution pseudodata (with 1.5% statistics), first with the amplitude γ_{12} fixed at 0 and then with γ_{12} fixed at 0.2 MeV$^{1/2}$. (b) Relative differences in cross sections from an R-matrix analysis of the elastic scattering angular distribution pseudodata at the four energies $E_\alpha=3451$, 5251, 5819, and 6258 keV (solid, short-dashed, long-dashed, and dotted curves, respectively) for the same conditions as in (a).

the pseudodata for each value of the reduced width.[12]

The figures show that the width of the $J^\pi=2^+$ subthreshold state influences points throughout the energy range, but most strongly above the narrow 2^+ resonance for the absolute differences. For the relative differences, however, the greatest effect is at the lowest energies. Typically, substantial changes in the widths of subthreshold states result in phase-shift differences of a fraction of a degree or cross section differences of about a millibarn (0.1–1.0 %). Most importantly, differences in cross section are most pronounced at angles smaller than 90° while scattering into the backward hemisphere seems to be in many cases relatively insensitive to the subthreshold widths.

We conclude that the reduced width amplitude γ_{12} can be deduced from elastic scattering data with the astrophysically desired precision, in particular with the now available ^{16}N data, if the systematic errors in the elastic scattering measurements can be reduced considerably compared with Ref. [13] and the statistics preferably improved. The reduced width amplitude γ_{11} derived from the ^{16}N data could be used in such a measurement as a consistency check.

C. Other experiments to restrict important reduced widths

For the determination of the $E2$ component of the radiative capture, it may be possible to restrict the reduced α width of the 6.92 MeV state in ^{16}O by other means, e.g., by using the β-delayed proton decay of ^{17}Ne into unbound states of ^{16}O as recently proposed in Ref. [29]. If we make the assumption that at least the ratio of the reduced α widths, γ_{11}/γ_{12}, can be determined, we simulate the restrictions imposed by this determination by doing fits to the radiative capture angular distribution data [24,8,9,11] and the β-delayed α spectrum of ^{16}N [12]. Elastic data were excluded for the reasons given above (Sec. IV). The result is Fig. 17, showing χ^2 versus $S_{E2}(300)$ with the ratio of the reduced width amplitudes, γ_{11}/γ_{12}, fixed at 0.51 (the weighted best value from Sec. V C). Any uncertainty in γ_{11}/γ_{12} will cause shifts in the parabola from which this additional error on $S(300)$ can be evaluated.

[12]In Ref. [13] a similar figure (Fig. 2) is shown with a much larger variation of phase shifts for different subthreshold reduced widths ($\theta^2_{\alpha,12}$). No reminimizations of other R-matrix parameters were performed for this figure. However, much smaller differences than shown in Fig. 2 of Ref. [13] are expected in the analysis of elastic scattering experiments since parameter correlations and limited statistical precision will substantially reduce the observable effects of subthreshold states.

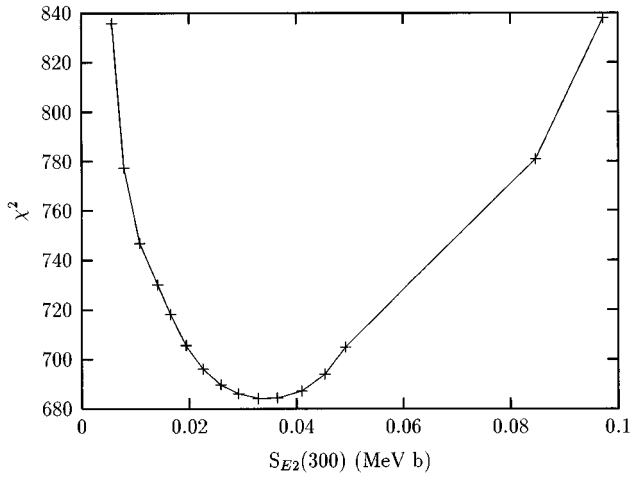

FIG. 17. χ^2 versus $S_{E2}(300)$ for the fixed ratio $\gamma_{11}/\gamma_{12}=0.51$ at $a=5.5$ fm.

We conclude that, if γ_{12}, the subthreshold state reduced α-width amplitude in the $\ell=2$ radiative capture of $^{12}C(\alpha,\gamma)^{16}O$, or (less stringently) γ_{11}/γ_{12}, its ratio to the width of the subthreshold 7.12 MeV state, can be restricted by any experiment, the cross section factor $S_{E2}(300)$ can be as well.

V. ADDITIONAL ASPECTS OF $^{12}C(\alpha,\gamma)^{16}O$

A. Reduced widths and transfer reactions

There have been many attempts to estimate the reduced α widths involved in the $^{12}C(\alpha,\gamma)^{16}O$ reaction from studies of α-transfer reactions [3,30–37]. In general, dimensionless reduced α widths are connected to the reduced width amplitudes $\gamma_{\lambda\ell}$ of the R-matrix theory[13] via [17]

$$\theta^2_{\lambda\ell,\alpha}=\frac{2\mu a^2\gamma^2_{\lambda\ell}}{3\hbar^2}=0.0479a^2\gamma^2_{\lambda\ell}, \tag{17}$$

with a in fermi and $\gamma^2_{\lambda\ell}$ in MeV. The results obtained for $\gamma_{\lambda\ell}$ in different experimental analyses are, however, dependent on the potentials used or implied in the analysis of the reaction data.

B. Reduced widths in the $E1$ radiative capture

As we have found significant systematic error effects resulting from the elastic scattering angular distribution and phase-shift data, particularly with respect to the reduced widths of the subthreshold states, we have excluded them from the further analysis presented here. This new R-matrix analysis includes all the experimental radiative capture angular distributions and the ^{16}N data as detailed above, but incorporates only one 3^- state fed by ^{16}N as was done in previous work [12]. The analysis was carried out for values of the radius parameter a ranging from 4.5 to 7.5 fm. The reduced width $\theta^2_{11,\alpha}$ for the subthreshold state at 7.12 MeV in ^{16}O was evaluated with Eq. (17) and the results are presented in Table III. It is obvious that the reduced width deduced from the fits does not stay constant with the interaction radius a, but rather closely follows a power law as a function of a. Because we do not know the reason for this dependence on the interaction radius a, we caution against a model-independent use of the reduced α width $\theta^2_{11,\alpha}$. In addition the reduced width found, in particular around $a=5.5$ fm (the interaction radius usually used in the previous literature), is considerably lower than those derived earlier (see, e.g., [3], Table 7.3).

TABLE III. Reduced α width $\theta^2_{11,\alpha}$ for the $E_x=7.12$ MeV state in ^{16}O using γ-capture data and the ^{16}N α spectrum in the fits.

a (fm)	4.5	5.0	5.5	6.0	6.5	7.0	7.5
$\theta^2_{11,\alpha}$	0.15	0.081	0.041	0.022	0.013	0.0073	0.0045

C. Transfer reactions and reduced widths for the $E2$ capture

Alpha-particle transfer reactions using lithium ions on ^{12}C have been used to extract spectroscopic information about the states in ^{16}O relevant to $^{12}C(\alpha,\gamma)^{16}O$ [30–37]. Problems in the determination of reduced widths by these transfer reactions arise from the separation of direct and compound components (the latter being particularly significant here), the model dependence of the results using different approaches to the distorted-wave Born approximation (DWBA) theory, structural uncertainties for specific states (node numbers), and the difficulties in determining backgrounds from higher-lying states in the case of broad structures like the 9.6 MeV state of ^{16}O. In general, it is possible that ratios of reduced widths are more reliably extracted from the transfer reaction information than absolute reduced widths, e.g., by eliminating energy-independent reflection factors arising from particular choices of nuclear potential as, e.g., discussed in Ref. [39] and references therein, thus reducing some of the systematic problems. However, the results of such ratio measurements which are shown in Table IV still exhibit a considerable experimental spread.

Calculations of reduced widths for these α-transfer results have been performed only for interaction radii close to $a=5.5$ fm. Comparison with Table IV shows that the ratios of $\theta^2_\alpha(7.1)/\theta^2_\alpha(9.6)$ do not agree well with the value $\theta^2_\alpha(7.1)/\theta^2_\alpha(9.6)\sim 0.1$ at $a=5.5$ fm obtained in our work even if one takes the necessary correction factor $(1+\gamma^2_{\lambda\alpha}\, dS/dE)$ into account [38].

It has also been argued [34,37] on the basis of angular distributions that the compound fraction in $^{12}C(^6Li,d)^{16}O$ is larger than in $^{12}C(^7Li,t)^{16}O$ and that the $(^6Li,d)$ data are therefore less reliable. However, again because no clear energy dependence is obvious for $^{12}C(^6Li,d)^{16}O$, where one would assume a diminishing compound fraction at higher energies, we take as our final estimate the entire range of values, i.e., $\theta^2_\alpha(7.1)/\theta^2_\alpha(6.9)$ ranging from 0.10 to 1.7.

This range of ratios of the reduced α widths has been used in fits to the experimental $^{12}C(\alpha,\gamma)^{16}O$ radiative capture angular distribution and the ^{16}N data, for $a=5.5$ fm. A range of $S_{E2}(300)$ from 9 to 92 keV b was found. We have varied a, keeping the ratio of reduced α widths fixed, and find slightly lower values of $S_{E2}(300)$ for small a and

[13]See footnote 4.

TABLE IV. Compilation of ratios of reduced α widths of E_x=6.9, 7.1, and 9.6 MeV states in ^{16}O for different references (Loeb-67 [30], Pühl-70 [31], Cob-76 [32], Cun-78 [33], Bec-78/1 [34], Bec-78/2 [35], Bec-80 [36], Bec-89 [37]).

Reference	Loeb-67	Pühl-70	Cob-76	Cun-78	Bec-78/1	Bec-78/2	Bec-80	Bec-89
Reaction	^{6}Li(^{12}C,d)	^{12}C(^{7}Li,t)	^{12}C(^{7}Li,t)	^{12}C(^{6}Li,d)	^{12}C(^{7}Li,t)	^{12}C(^{6}Li,d)	^{12}C(^{6}Li,d)	^{12}C(^{7}Li,t)
$E_{\rm lab}$(MeV)	18–24	15–24	38	20–34	34	42.1	90.2	70/101
$\frac{\theta_\alpha^2(7.1)}{\theta_\alpha^2(9.6)}$ [a]	[b]	[b]	[b]	[b]	0.35 ± 0.13	$0.6^{+1.7}_{-0.3}$	0.3-0.6[c]	0.35 ± 0.07
$\frac{\theta_\alpha^2(7.1)}{\theta_\alpha^2(6.9)}$	0.48 ± 0.24	0.14[d]	0.18[d]	1.70[d]	0.30[d,e] 0.21[d,e]	0.53[d] 0.24[d]	0.1-0.4[c]	0.17 ± 0.05

[a]To compare to values derived with the R matrix a correction factor given by the ratios of $1+\gamma^2_{\lambda\alpha}\, dS/dE$ (here 0.68) has to be applied. This correction [38] was not included in Refs. [34–37].

[b]Not determined.

[c]Range given in Bec-80. From finite-range distorted wave (FRDW) calculations, discussed in the same article, ratio values of 0.7 and 0.4 are found.

[d]No errors quoted.

[e]From Bec78/2, two other combinations of ratios possible.

slightly higher values for larger interaction radii a.

In summary, we first note that the analysis of the elastic scattering angular distributions should have given the most stringent constraints on $S_{E2}(300)$. Because of the systematic problems found there, we are, however, not confident of the results derived by including the elastic scattering data. In the case of the α-transfer reactions quoted above, concerns about the model dependence of α-transfer reactions and the present uncertain state of the theory connecting α-transfer reactions and R-matrix analyses imply that similar caution should be exercised with regard to the reduced widths deduced from α-transfer experiments.

D. Theoretical models

As the subthreshold 2^+ state has a well-established (4p-4h) structure [40], it has long been recognized that the $E2$ part of the low-energy ^{12}C(α,γ)^{16}O cross section should be well described by $\alpha+^{12}$C cluster models. In fact, cluster model studies with varying degrees of sophistication have been employed to calculate $S_{E2}(300)$. These studies include microscopic single-channel and multichannel generator-coordinate method (GCM) calculations as in Refs. [41–43], microscopic potential-model calculations [28,9,44], and folding potential model calculations [46]. In contrast with the microscopic GCM and potential models, which allow consistent descriptions of the scattering states (including the subthreshold 2^+ level) and the ^{16}O ground state within the same model space, the folding potential model requires the introduction of *ad hoc* spectroscopic factors, taken inconsistently from outside the model, to compensate for the fact that the ^{16}O ground state is not well described by nonantisymmetrized $\alpha+^{12}$C cluster wave functions.

The microscopic GCM and potential model calculations were based on harmonic-oscillator many-body wave functions with identical oscillator parameters b for the clusters. The Pauli-forbidden states, which induce the nodal structure in the relative wave functions and generally influence capture cross sections quite sensitively [45], are then given by harmonic oscillator states with width b/μ, where μ is the reduced mass parameter. The restriction of identical cluster parameters has been overcome [47] within a multichannel orthogonal condition model (OCM) calculation based on antisymmetrized $\alpha+^{12}$C(0^+,2^+,4^+) cluster wave functions (including the first 0^+, 2^+, and 4^+ states in ^{12}C) with different and realistic size parameters for the α particle and the ^{12}C nucleus. This calculation yields a remarkably good description of the low-energy ^{16}O properties. We note that this calculation gives a slightly different energy dependence of the S_{E2} factors from the other calculations, which, however, is in nice agreement with the $E2$ data derived here from Ref. [11] (see Fig. 2). At the astrophysically most effective energy the calculation in Ref. [47] predicts $S_{E2}(300)=70$ keV b.

All of these models, if tuned to physically relevant input, predict $S_{E2}(300)$ in the range 50–100 keV b (for a compilation see Refs. [43,48]). Furthermore, predictions of these models also agree rather well with the energy dependence of $S_{E2}(E)$ for $E<2.5$ MeV (see Fig. 2).

VI. CONCLUSION

We summarize the conclusions derived in the preceding sections in the analysis of the present experimental data.

(i) The S factor for the $E1$ capture is stable under all fitting conditions at 80 keV b. We therefore adopt the value of Ref. [12] which also includes estimates of systematic errors in all of the measurements concerned.

(ii) With the phase shifts of Ref. [13], the radiative capture data, and the ^{16}N data, the S factor for the $E2$ capture at 300 keV is not constrained very well; we estimate 140 keV b to be a cautious upper limit for $S_{E2}(300)$.

(iii) Alternatively, with the inclusion of the elastic scattering angular distributions of Ref. [13], restrictions are obtained which limit $S_{E2}(300)$ to <35 keV b, with the χ^2 mini-

mum at 13 keV b. However, the elastic data of [13], taken by themselves, lead to a minimum of χ^2 with both the $E1$ and the $E2$ subthreshold α widths close to zero, which, for the $E1$ part, is in direct contradiction with the result from the ^{16}N α spectrum. There is also an inconsistency with the f-wave subthreshold state strength. In addition, there are experimental problems with the target thickness and the normalization of cross sections. We are therefore not prepared to accept the results of fits to these elastic scattering data as reliable.

(iv) Both theoretical predictions on $S_{E2}(300)$ and α-transfer reaction analyses yield results which are within the broad range of values derived here. However, both of these approaches have uncertainties with magnitudes that remain unknown.

In the determination of the total cross section for the $^{12}C(\alpha,\gamma)^{16}O$ reaction, cascade transitions have to be included. For the cascade transitions it is found that the unobserved $E2$ direct capture into the $J^\pi=0^+$ state at 6.05 MeV of ^{16}O is likely to be the most prominent cascade transition with an estimated S factor $S_{E2}^{6.05}(300)$ of 9 keV b [43]. The direct capture into the 6.92 MeV state of ^{16}O has been estimated [9] to be 7 keV b at 300 keV, while the direct capture to the 7.12 MeV state probably contributes very little (0.3 keV b) at 300 keV. These results are highly uncertain, but they do not constitute a large fraction of the cross section.

Our final value for the total S factor is therefore 62 keV b $\leqslant S(300) \leqslant$ 270 keV b , where the lower limit corresponds to $S_{E1}(300)=58$ keV b, $S_{E2}(300)=4$ keV, with zero cross section for the cascade transitions. The upper limit is given by $S_{E1}(300)=100$ keV b, $S_{E2}(300)=140$ keV, with 30 keV b for the cascade transitions. The lower limit of 4 keV b for $S_{E2}(300)$ corresponds exclusively to the direct capture part of the $E2$ radiative capture. An alternative way to express the currently available S- factor information is the (quadratic) sum of the ground state $E1$ and $E2$ S factors, and the cascade-transition S factors; i.e., $S_{E1}(300)=79\pm21$ keV b, $S_{E2}(300)=70\pm70$ keV b, and $S_C(300)=16\pm16$ keV b, which gives $S(300)=165\pm75$ keV b.

Through the simulation of possible future experiments we conclude that a remeasurement of elastic α scattering with the statistical accuracy of Ref. [13] can restrict $S_{E2}(300)$ to a significant precision, as is already apparent from the analysis of the data of Ref. [13], providing that systematic errors can be substantially reduced as compared with the existing data. Better restrictions on $S(300)$ in $^{12}C(\alpha,\gamma)^{16}O$ by improving radiative capture data will require greatly improved data. Because real experiments introduce systematic errors that have to be included in addition to the statistical errors simulated here, it is very unlikely, in our opinion, that an $S(300)$ value with an error significantly smaller than 30% will be forthcoming in the foreseeable future.

ACKNOWLEDGMENTS

The authors are grateful to the Queen's University group, in particular Prof. H. Evans, for making their primary data available before publication. The authors also wish to thank Dr. U. Giesen and Dr. C. Iliadis for their contributions to discussions of transfer reactions. We also wish to express our gratitude to Prof. E.W. Vogt for his extensive discussions of R-matrix theory and transfer reactions. We would like to thank Prof. C. Rolfs of Bochum University for comments on the manuscript. The work has been partially supported by the Natural Sciences and Engineering Research Council of Canada, and by Grants Nos. PHY 94-20470 and PHY 94-12818 from the U.S. National Science Foundation.

[1] W.A. Fowler, Rev. Mod. Phys. **56**, 149 (1984).
[2] T.A. Weaver and S.E. Woosley, Phys. Rep. **227**, 65 (1993).
[3] C.E. Rolfs and W.S. Rodney, *Cauldrons in the Cosmos* (University of Chicago Press, Chicago, 1988), p. 387.
[4] M. Hashimoto, Prog. Theor. Phys. **94**, 663 (1995).
[5] R.J. Jaszczak, J.H. Gibbons, and R.L. Macklin, Phys. Rev. C **2**, 63 (1970).
[6] R.J. Jaszczak and R.L. Macklin, Phys. Rev. C **2**, 2452 (1970).
[7] P. Dyer and C.A. Barnes, Nucl. Phys. **A233**, 495 (1974).
[8] K.U. Kettner, H.W. Becker, L. Buchmann, J. Görres, H. Kräwinkel, C. Rolfs, P. Schmalbrock, H.P. Trautvetter, and A. Vlieks, Z. Phys. A **308**, 73 (1982).
[9] A. Redder, H.W. Becker, C. Rolfs, H.P. Trautvetter, T.R. Donoghue T.C. Rinkel, J.W. Hammer, and K. Langanke, Nucl. Phys. **A462**, 385 (1987).
[10] R.M. Kremer, C.A. Barnes, K.H. Chang, H.C. Evans, B.W. Fillipone, K.H. Hahn, and L.W. Mitchel, Phys. Rev. Lett. **60**, 1475 (1988).
[11] J.M.L. Ouellet, H.C. Evans, H.W. Lee, J.R. Leslie, J.D. McArthur, W. McLatchie, H.-B. Mak, P. Skensved, J.L. Whitton, X. Zhao, and T.K. Alexander, Phys. Rev. Lett. **69**, 1896 (1992).
[12] R.E. Azuma, L. Buchmann, F.C. Barker, C.A. Barnes, J.M. D'Auria, M. Dombsky, U. Giesen, K.P. Jackson, J.D. King, R.G. Korteling, P. McNeely, J. Powell, G. Roy, J. Vincent, T.R. Wang, S.S.M. Wong, and P.R. Wrean, Phys. Rev. C **50**, 1194 (1994).
[13] R. Plaga, H.W. Becker, A. Redder, C. Rolfs, H.P. Trautvetter and K. Langanke, Nucl. Phys. **A465**, 291 (1987); R. Plaga, diploma thesis, University of Münster, 1986.
[14] C.M. Jones, G.C. Philips, R.W. Harris, and E.H. Beckner, Nucl. Phys. **37**, 1 (1962).
[15] G.J. Clark, D.J. Sullivan, and P.B. Treacy, Nucl. Phys. **A110**, 481 (1968).
[16] F. Ajzenberg-Selove, Nucl. Phys. **A471**, 1 (1987); D.R. Tilley, H.R. Weller, and C.M. Ceves, *ibid.* **A564**, 1 (1993).
[17] F.C. Barker and T. Kajino, Aust. J. Phys. **44**, 369 (1991).
[18] R.G. Thomas, Phys. Rev. **88**, 1109 (1952).
[19] F.C. Barker, Aust. J. Phys. **24**, 777 (1971).
[20] A.M. Lane and R.G. Thomas, Rev. Mod. Phys. **30**, 257 (1958).
[21] J. Humblet, B.W. Filippone, and S.E. Koonin, Phys. Rev. C **44**, 2530 (1991).
[22] J. Humblet, Phys. Rev. C **42**, 1582 (1990).
[23] B.W. Filippone, J. Humblet, and K. Langanke, Phys. Rev. C **40**, 515 (1989).

[24] P. Dyer, Ph.D. thesis, Caltech, 1974.
[25] K. Neubeck, H. Schober, and H. Wäffler, Phys. Rev. C **10**, 320 (1974); H. Hättig, K. Hünchen, and H. Wäffler, Phys. Rev. Lett. **25**, 941 (1970).
[26] Z. Zhao, R.H. France III, K.S. Lai, S.L. Rugari, M. Gai, and E.L. Wilds, Phys. Rev. Lett. **70**, 2066 (1993).
[27] ''MINUIT, Function Minimization and Error Analysis,'' CERN Program Library Entry D506 (unpublished).
[28] K. Langanke and S.E. Koonin, Nucl. Phys. **A439**, 384 (1985).
[29] J. King, R.E. Azuma, L. Buchmann, J.M. D'Auria, M. Dombsky, U. Giesen, C. Iliadis, K.P. Jackson, A.C. Morton, J. Chow, G. Roy, W. Galster, A. Shotter, T. Davinson, and R.N. Boyd, Proposals to the TRIUMF Experiment Evaluation Committee, 1994 and 1995 (unpublished).
[30] H.M. Loebenstein, D.W. Mingay, H. Winkler, and C.S. Zaidins, Nucl. Phys. **A91**, 481 (1967).
[31] F. Pühlhofer, H.G. Ritter, G. Bock, G. Brommundt, H. Schmidt, and K. Bethge, Nucl. Phys. **A147**, 258 (1970).
[32] M.E. Cobern, D.J. Pisano, and P.D. Parker, Phys. Rev. C **14**, 491 (1976).
[33] A. Cunsolo, A. Foti, G. Pappalardo, G. Raciti, and N. Saunier, Phys. Rev. C **18**, 856 (1978).
[34] F.D. Becchetti, E.R. Flynn, D.L. Hanson, and J.W. Sunier, Nucl. Phys. **A305**, 293 (1978).
[35] F.D. Becchetti, J. Jänecke, and C.E. Thorn, Nucl. Phys. **A305**, 313 (1978).
[36] F.D. Becchetti, D. Overway, J. Jänecke, and W.W. Jacobs, Nucl. Phys. **A344**, 336 (1980).
[37] F.D. Becchetti, M.L. Dowell, P.M. Lister, J.W. Jänecke, A. Nadasen, and J.S. Winfield, Proceedings of the Fifth International Conference on Clustering Aspect in Nuclear and Subnuclear Systems, Kyoto [J. Phys. Soc. Jpn. **58**, 635 (1989)].
[38] E.W. Vogt (private communication).
[39] E.W. Vogt, G. Michaud, and H. Reeves, Phys. Lett. **19**, 57 (1965).
[40] G.E. Brown and A.M. Green, Nucl. Phys. **75**, 401 (1966).
[41] P. Descouvemont, D. Baye, and P.H. Heenen, Nucl. Phys. **A430**, 426 (1984).
[42] P. Descouvemont and D. Baye, Phys. Rev. C **36**, 1249 (1987).
[43] P. Descouvemont, Phys. Rev. C **47**, 210 (1993).
[44] C. Funck, K. Langanke, and A. Weiguny, Phys. Lett. **152B**, 11 (1985).
[45] D. Baye and P. Descouvement, Ann. Phys. (N.Y.) **165**, 115 (1985).
[46] H. Krauss *et al.* in *Nuclei in the Cosmos*, edited by H. Oberhummer and W. Hillebrandt (MPI für Physik und Astrophysik, Garching, 1990).
[47] S. Okabe, in Proceedings of the Conference on Cluster Physics, Strasbourg, 1994 (unpublished).
[48] K. Langanke and C.A. Barnes, in *Advances in Nuclear Physics*, edited by J.W. Negele and E. Vogt (Plenum Press, New York, 1996), Vol. 22, p. 173.